Plasma Impedance: "The end of the line?"

Thesis

Plasma Impedance

" The end of the line? "

Jonathan Moore

A thesis submitted in partial fulfilment of the requirements of the Open University for the Degree of Master of Philosophy

July 1998

DATE OF SUBMISSION: 14 JULY 1998
DATE OF AWARD: 4 JANUARY 1999

The Open University
Oxford Research Unit, Foxcombe Hall
Oxford, OX1 5HR

Acknowledgement

I would particularly like to acknowledge the help and encouragement of my supervisor Dr. Nicholas Braithwaite who has led, nay teased me into the practice of "Armchair Analysis" and in doing so has left his mark! Thank you.

Thanks are also due to associates and technical staff at the research unit for their support and, on many occasions, patience – it could not have been easy.

A final mention should go to Mr. Charlie Mahony at Queens University, Belfast for making my visit so beneficial and enjoyable. I cannot think of a more beautiful city in which to have worked and played so hard!

Contents

1. Abstract

This report accompanies the research performed during the first three terms of a one-year MPhil program into RF-generated, capacitively-coupled gas discharge plasmas and methods of electrical diagnostics.

Gas discharge plasmas are often used for surface processing in the semiconductor fabrication industry and a discharge's electrical properties (power and impedance) are often required to be related to its physical and chemical mechanisms. Typical R.F supplies do not incorporate accurate enough power monitors with even fewer indicating impedance. Even so, it is required to measure power and impedance *actually* at the driven electrode and not prior to a lossy matching network and chamber feed.

The design and calibration of an accurate voltage and current probe are proposed (to be placed at a point between the matching network and the discharge chamber) together with a procedure to fully characterise the transmission line that remains between the probe and electrode.

Finally, a software routine is presented to indicate power and impedance together with distortion of the 2^{nd} and 3^{rd} harmonic, feed efficiency and various equivalent circuits. Results show that the proposed probe is of reasonably high accuracy and that measurements taken of typical plasma discharges relate to theory in the main.

2.Background

2.1. Uses of plasma technology

Modern society finds much use for the application of gas discharges in the development of various technologies. These are wide ranging, from simple lamps for cost effective lighting to those of ambitious complexity such as those proposed for nuclear fusion.

Industrial Application

The semiconductor and material processing industries are the main users of low temperature plasma discharges as it allows them to produce microscopic changes to a material's surface. This could be thin film deposition, for example metallizing a surface, or the defining of features by ion etching which is far superior to chemical etching, allowing higher density microchips.

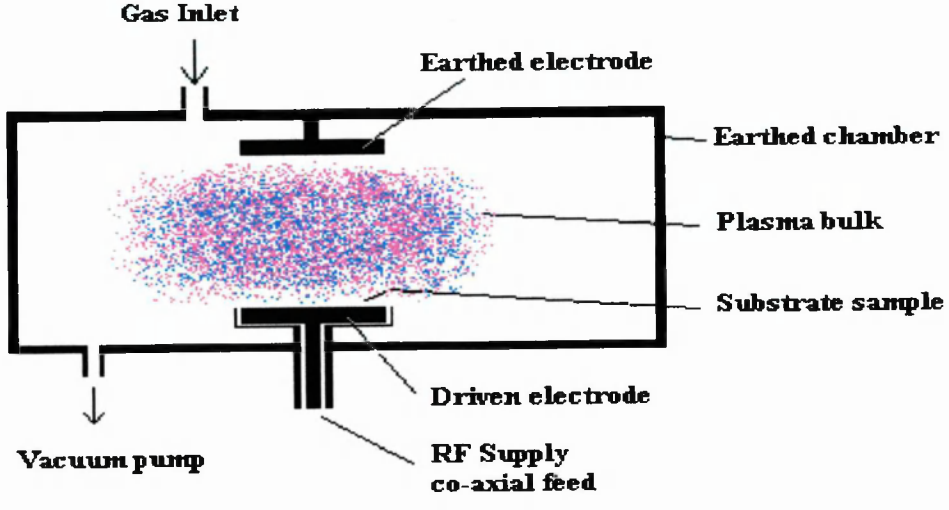

Figure 1. Typical argon discharge chamber for use in surface processing.

A vacuum chamber is filled with various gases at low pressure and excited with either DC or AC power. The gas becomes weakly ionised and reaches an equilibrium state about its immediate environment. The chamber is earthed and has a powered electrode inside in order to excite the gas molecules. A sheath is formed around the electrode (driven and earthed) and the chamber with the 'bulk' of the plasma in the centre. This sheath is a space charge region caused by the difference in the bulk and the electrodes' potential. The bulk contains both electrons and ions and these ions will be attracted to (and accelerated towards) the lower DC potential of the powered electrode. Electrons may approach this electrode but will be repelled away at a point where their kinetic energy is reduced to zero due to the opposing force. For a collisionless sheath (no ionisation) only very high energy electrons will reach the electrode, thus reducing its potential further. Characteristics of this sheath region are the main area of interest when controlling and modifying the chemistry of the surface interactions.

For surface processing, a substrate (for example, a silicon wafer) is attached to either the powered or earthed electrode, which can then be bombarded with a particular choice of ions. The higher the potential of the plasma the more energy an ion will have and controlling the plasma potential is therefore very useful in determining etch rates for example.

Commercial Application

Plasma technology is also found in various commercial applications, in particular visual displays. This will vary from neon and fluorescent lighting to the most advanced flat screen displays as used in lap top computers and new generation television screens. FST (Flat Screen Television) displays are under continual development as the demand and market would appear to be huge.

2.2. Why measure plasma impedance and power?

Impedance and power are two parameters that will completely characterise, what is effectively, a one port network and hence the electrical behaviour of a particular system can be determined and utilised for either process diagnostics or to further academic understanding.

Industry

Plasma power measurement in industry is invaluable to chamber and feed system design. It is important that power transfer from the generator into the gas discharge is as efficient as possible. Main causes of loss will be the matching network itself (owing to the finite coil resistance), chamber feed system and the associated feed from the generator.

A typical use of impedance monitors is to aid in the detection of process changes, in particular end point detection in an etching system. For instance, the impedance will change considerably when the plasma has etched away the silicon dioxide to then reach the silicon wafer and so monitoring this parameter is important to adjusting a process's recipe (gas mixtures and etch times etc).

Studies show that the phase angle of impedance is sensitive to the nature of gases in the chamber [1]. It is possible therefore, in principle, to use this diagnostic as a type of leak detector, which could then be used to trigger various types of safety procedure or for detecting other compositional changes.

Research

Power and impedance measurements are an invaluable diagnostic tool that can be performed externally by (what are approaching) non-invasive methods. Most of a plasma's physical and chemical processes are related to the impedance (and hence power). For example, plasma density and sheath dimensions are related to real loss and capacitance respectively.

Cross comparison amongst research in plasma science can use impedance measurements to confirm, and ensure, similarities in the behaviour of seemingly identical systems. A typical case being the GEC (Gaseous Electronics Conference) reference cell as proposed by J.K.Olthoff et. al. [2]

It is important to distinguish between the impedance of the discharge itself and the impedance of the entire load circuit. We need to know the instantaneous voltage on the RF driven electrode and the current that is flowing at that point, together with the phase relationship between the two. The measurement has to take place outside of the cell and therefore the transfer function between the measurement point and the driven electrode needs to be known. In practice, the minimum circuit to characterise would be the main feed into the system i.e. a capacitive driven electrode and some series inductance and loss. The detection of the voltage and current is then made in series with a typical coaxial feed.

The project can therefore be split into two main areas, firstly the theory and development of a so-called 'VI Probe' and secondly the modelling of the complete system to determine the probe's ideal placement, together with problems relating to this and the subsequent transfer functions that are required.

2.3. What to expect

In order for the system to be considered in relation to designing the VI probe and in terms of general safety, an estimate of the magnitude of voltages and currents likely to be present in a typical laboratory application is needed.

Typical powers indicated by the RF supply depend on the application, but in this case vary up to a maximum of perhaps 300W. Assuming a plasma presents a load in the region of 50Ω then voltage will be about $120V_{rms}$. Current in this case would be about $2.5A_{rms}$. The effect of resonances within the matching network and at other points in the system could mean that voltages would be higher than that suggested but it is still unlikely that there will be problems with potential breakdown or conductor current capability.

It should be noted here that even low voltages at RF frequencies can be considered a serious burn and shock hazard, therefore precaution was taken at all times during experiments on live apparatus.

3. The Voltage & Current Probe

3.1. General Theory

The voltage and current probe is a calibrated device that couples appropriate signals from a basic transmission line feed (to the device being measured) and converts them into voltages that represent the voltage on that line together with the current flowing along it. Ideally the device would be entirely non-invasive but this is not possible due to energy being coupled into our measurement voltages. The only practical solution is to couple minuscule amounts of energy and thereby minimise the probe's effect.

Voltage Measurement

Voltage measurements are made by capacitively coupling to the main feed line. This is achieved by loading the feed with a small capacitance and a resistance in series. The current in a capacitor is proportional to the rate of change of the voltage applied.

$$i = C\frac{\mathrm{d}V}{\mathrm{d}t} \qquad 1$$

If the capacitance, resistance and frequency are held constant then the voltage developed across the resistor (i/R) will be proportional to the level of AC signal on the line. The phase of this voltage will be approximately in phase with respect to the feed line voltage if $\omega CR >> 1$.

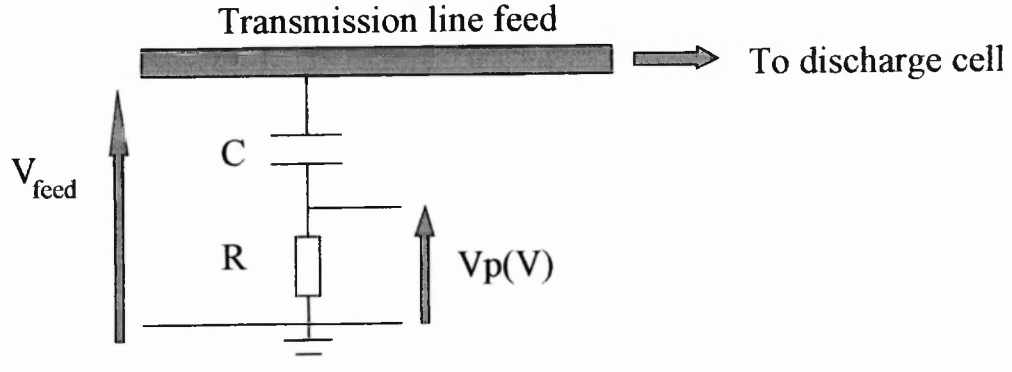

Figure 2. Circuit diagram of voltage probe.

$$\frac{V_p(V)}{V_{feed}} = \frac{\mathrm{j}\omega CR}{1+\mathrm{j}\omega CR} \qquad 2$$

If ωCR is a lot less than 1 then we can approximate that the transfer function is directly proportional to frequency.

$$\frac{V_p(V)}{V_{feed}} = j\omega CR \qquad 3$$

In practice the resistance R is chosen to be the characteristic impedance of the line terminated by the oscilloscope and the capacitance is implemented by a small cylindrical tube around a circular feed line (separated by a PTFE dielectric sleeve of permitivity, $\varepsilon_r \approx 2.1$). It can be shown that capacitance of this structure is approximately $\varepsilon_o \varepsilon_r 2 \pi r l / d$ where r is the internal radius to the inside of the metallic sleeve, l is sleeve length and d is the thickness of the insulator. C is calculated to be in the region of 3.5 picofarads. At a frequency of 13.56MHz we find that ωCR is about 0.015 and this suggests the above theory will hold true.

Current Measurement

Current is measured inductively by coupling from the main line into a terminated line. The voltage across an inductor is proportional to the rate of change of the current passing through it.

$$V = L\frac{di}{dt} \qquad 4$$

If the inductive coupling and resistance are constant together with the frequency then the voltage across the resistance (and the current through it) is proportional to the amount of current flowing through the line.

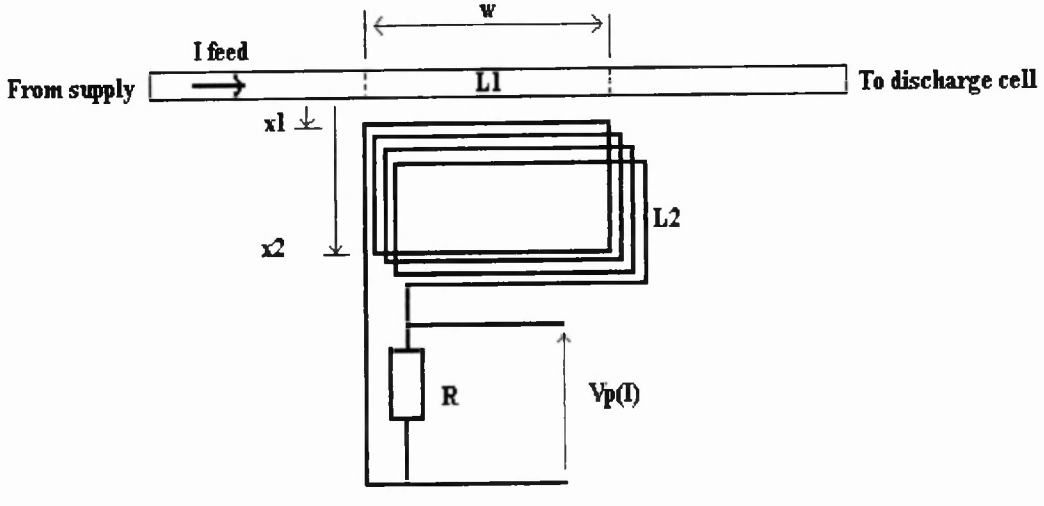

Figure 3. Circuit diagram of current probe.

The inductive sensor can be considered analogous to a T network of inductances to determine the relationship between I_{feed} and V_p *(I)*

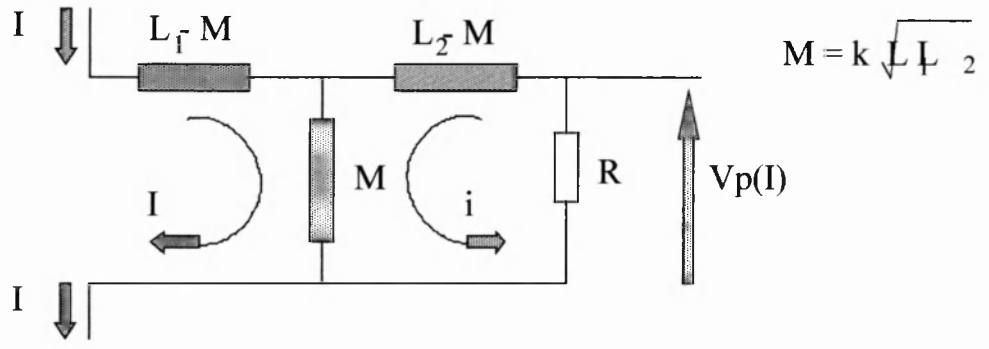

Figure 4. Electrical model of current probe.

Where: M = mutual inductance and k = coupling coefficient.

From Kirchoff we can see that:

$$(I+i)\mathrm{j}\omega M = -\mathrm{j}\omega(L_2 - M)i + V_p(I) \qquad \mathbf{5}$$

Where: $V_p\ (I) = i.R$

Therefore:

$$[I + \frac{V_p(I)}{R}]\mathrm{j}\omega M = V_p(I)[1 - \frac{\mathrm{j}\omega(L_2 - M)}{R}] \qquad \mathbf{6}$$

$$\mathrm{j}\omega M\, I = V_p(I)[1 - \frac{\mathrm{j}\omega(L_2 - M)}{R} - \frac{\mathrm{j}\omega M}{R}] \qquad \mathbf{7}$$

Therefore:

$$V_p(I) = \frac{\mathrm{j}\omega M\, I}{[1 - \frac{\mathrm{j}\omega L_2}{R}]} \qquad \mathbf{8}$$

If $\omega L_2 << R$ then the transfer function ($V_p(I)/I_{feed}$) would appear to be directly proportional to frequency (so-called differential probe). The arrangement used for this measurement consists of four turns of wire (L_2), a 50Ω resistor, and a 50Ω line terminated at the scope.

An estimate of L_2 and M will allow an approximate calculation for the transfer function, ωM, and determine how linear the function will be with relation to frequency i.e. at what frequencies is it considered to deviate from an ideal differential probe.

Estimating the coupling loop inductance, L_2

It can be shown that a square loop of dimensions X by Y metres and wire thickness R has an inductance given by:

$$L = \frac{\mu_o}{2\pi}\left[2Y\ln\left(\frac{X-R}{R}\right) + 2X\ln\left(\frac{Y-R}{R}\right)\right] \qquad \textbf{9}$$

Where μ_o is permeability, in this case, of free air (4π x 10^{-7} henry/metre)

L_2 can be approximated to $4L$ for four turns of wire. For R = 1.0mm, X = 20mm and Y = 10mm L_2 is in the region of 115nH.

Estimating mutual inductance

Mutual inductance is due to the magnetic flux that is developed in the main feed line cutting the current path of the inductor loop, L_2. Integrating the generated flux density over the area of the loop can show that the mutual inductance, M is given by:

$$M = \frac{\mu_0 w}{2\pi}\ln\left(\frac{x_2}{x_1}\right) \qquad \textbf{10}$$

Dimensions of the coupling inductor and its position in the Mk.1 design, as shown in figure 3 are approximately x_1 = 5mm, x_2 = 15mm and width, w = 20mm.

For a single turn of this inductive loop, M = 4.4nH therefore the prototype's four turn design can be estimated at 17.6nH.

Using equation 8, the current transfer function can now be estimated as 1.5/.8 = 1.86VA^{-1} (or 0.536AV^{-1}). Comparing this to the measured transfer function of the probe at 0.748AV^{-1} (see appendix C) indicates that this simple model is a reasonable approximation.

It can also be noted that, in this case, the current probe's transfer function deviates from that of an ideal differential probe by +25% at 13.56MHz. Although this is accounted for in the estimation and measurement, it suggests that the function is differential up to about 65MHz at which point a phase change occurs due to $\omega L_2/R$ being greater than 1.

3.2. Construction

A VI probe was built on the principles outlined in 3.1. It was housed in a die-cast aluminium box to screen and neatly hold the various parts and use N-type connectors for the main feed with BNC connectors for V, I and DC bias probes (see section 3.5).

The dimensions and internal arrangements are shown in figure 5.

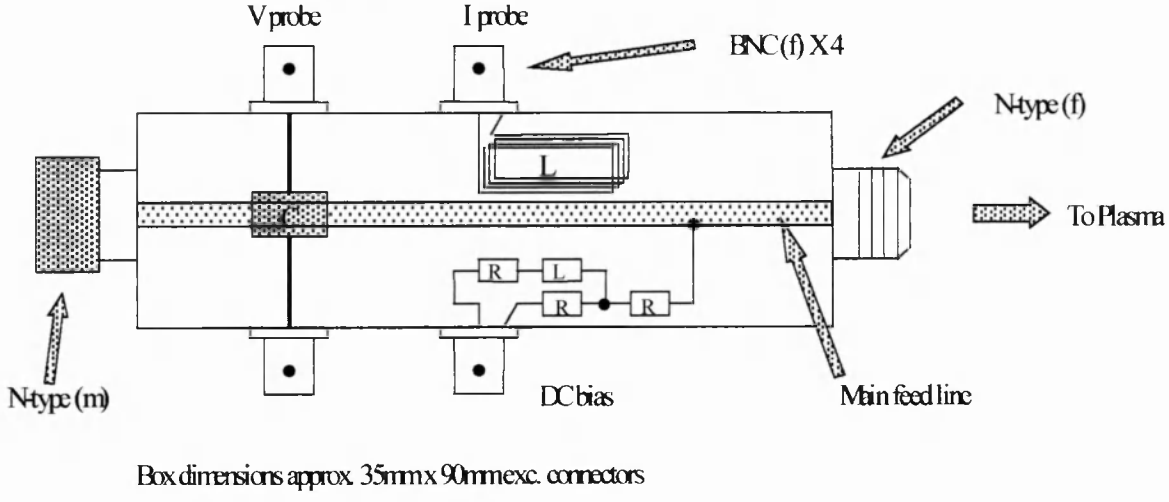

Figure 5. Construction of the VI probe.

There are two outputs for the voltage measurement purely to allow a more rigid support for the cylindrical capacitance. Either connector can be used but the other should not be loaded.

The DC bias output allows the DC voltage on the feed line to be measured. This can then be related to the plasma potential (voltage on the electrode) by taking account of the feed inductance and loss.

3.3. Calibration

In order to calibrate the VI probe, measurements (at the frequency of interest) are taken using a known wholly resistive load. A 50Ω resistor designed as a load for use in microwave circuits at up to 6GHz was obtained and connected to a launch. This load is manufactured by Florida R.F. Labs and has a specified VSWR (Voltage Standing Wave Ratio) of less than 1.3:1 at 6 GHz, 100W power rating and a tolerance of 5%.

At the relatively low frequencies used in these experiments the VSWR is generally very low with return losses of more than 30dB when connected in ideal conditions. This is achieved by mounting the resistor on an aluminium heatsink and using a 1.6mm thick PCB (FR4 type glass fibre material) with a 3mm wide track [3] to form a microstrip launch to a suitable connector (N-type female). See figure 6.

Figure 6. Pseudo-precision loads.

The entire calibration revolves around the fact that this load is indeed entirely real at 13.56MHz in order for the current and voltage to be known to be in phase.

Procedure

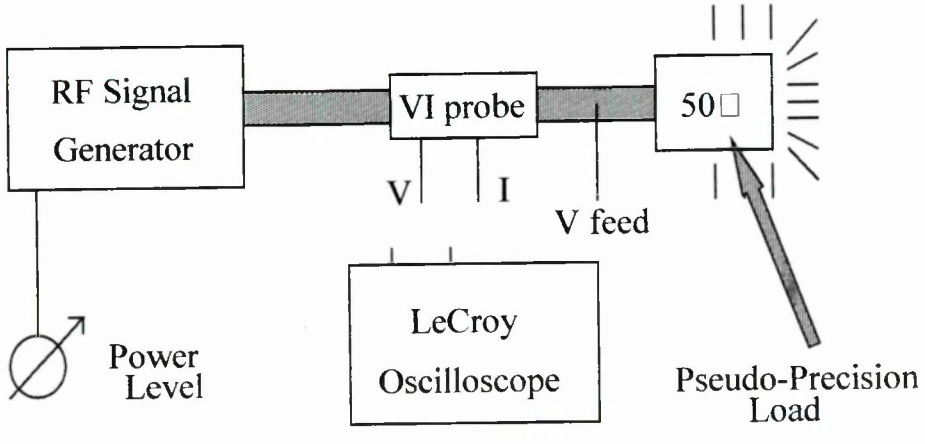

Figure 7. Calibration arrangement.

Purpose made BNC leads were used in the calibration and measurement procedures in order to keep any propagation delays associated with them accounted for.

In all cases the voltage and current transfer functions were measured at different power levels (10 to 85W) to check for any non-linear mechanisms.

The oscilloscope was adjusted to display with maximum resolution for all measurements as it was discovered that the quantisation errors (errors incurred through the digitisation process) could accumulate when the vertical sensitivity was not optimised. Each measurement is averaged over at least 100 periods (multiple shot averaging) and any possible display error is recorded and can be accounted for when calculating the propagation of errors (appendix A).

The probe leads were allocated colour labels to ensure consistency and both were terminated by the scope (50Ω DC coupled). A second, commercial probe was used to measure the voltage actually on the line. It was a LeCroy x10 10MΩ i/p impedance probe. Consistency with the measurements and routine were maintained throughout, e.g. comparing rms, peaks or peak to peaks. The waveforms measured appeared to be undistorted (purely fundamental) and therefore a measured voltage peak was taken as the amplitude of the fundamental.

The first measurement was of the voltage on the line, comparing the capacitively coupled probe to the commercial resistive divider probe. This gave a voltage transfer function. The current in the line was assumed to be in phase with the voltage on the line and related in amplitude by $I=V/R$ (where R is 50.40Ω - the DC resistance). This can then be compared to the voltage at the inductively coupled probe to obtain a current transfer function.

As well as these transfer functions being measured, the propagation delay between the V and I signals was noted at different nominal powers (the displayed forward power on the generator). For interest, the power in the test load was also calculated to compare with that displayed in the power supply metering.

3.4. V, I & θ Transfer functions

A summary of the measured transfer functions is shown below.

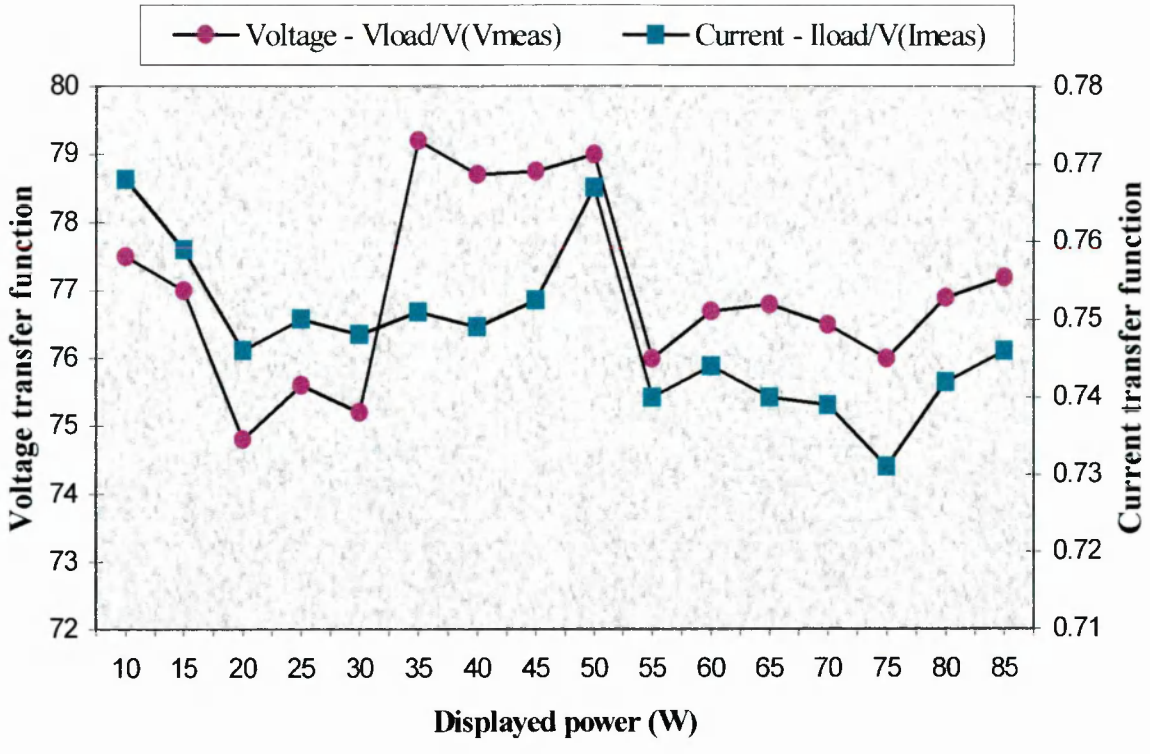

Figure 8. Voltage and Current transfer functions.

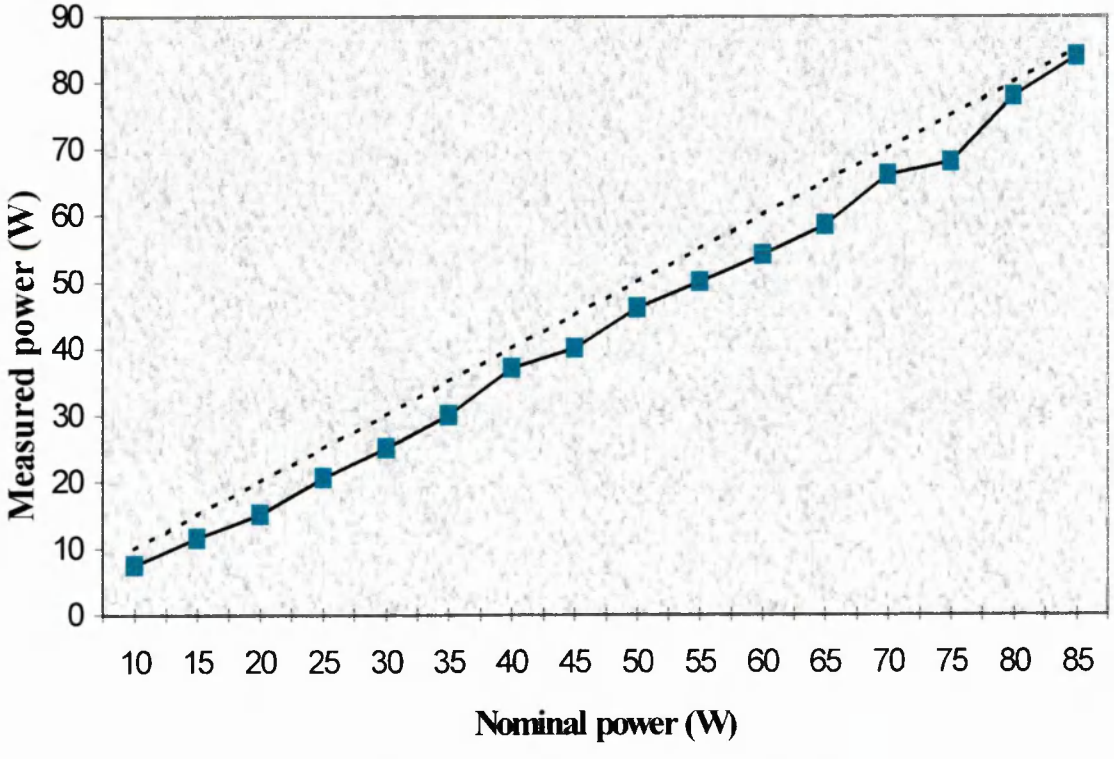

Figure 9. Measured as a function of nominal power.

It can be seen that the voltage and current transfer functions are far from constant, showing quite large deviations from the mean. They do however show similar trends suggesting that deviations were systematic to the calibration procedure. Mean values are $76.988VV^{-1}$ and $0.7482AV^{-1}$ for voltage and current functions respectively (i.e. 76.988 volts and 0.7482 amp for every volt measured at each probe). The corresponding maximum deviations from the mean are ~2 and ~0.02 or 2.6% and 2.7%. These are the maximum deviations measured and more realistic values can be determined from propagating the errors through calculations in the calibration/test measurements. An explanation of the theory behind this is given in appendix A. In summary, the mean and standard deviations of the transfer functions are:

$$V_{load}/V_{probe} = \mathbf{76.988} \text{ with } \delta = \mathbf{0.05125}$$
$$I_{load}/I_{probe} = \mathbf{0.7482} \text{ with } \delta = \mathbf{0.000577}$$

The results of measuring real power as a function of displayed power is encouraging and demonstrates the extent of global inconsistency in the measurements as being reasonably small (the deviation from a linear relationship – shown as a dashed line).

Propagation delay between the measured signals and those expected was very constant as a function of power and to a large extent frequency. With the unit orientated as mentioned in section 3.2, the current waveform is leading the voltage signal by 3.0ns. If the unit is installed in the other direction then the lead will be 3.0ns +180° = 3.0 + 73.7/2 = 39.85ns (where 73.7ns is the period at 13.56MHz).

3.5. DC bias measurement

As mentioned, a method of measuring the DC voltage on the feed line is required (which can then be related to the voltage on the electrode- section 4). The circuit used is a simple potential divider followed by a LCR filter. The network should load the feed as little as possible (high input impedance) and attenuate the RF signal as well as having a known constant DC transfer function.

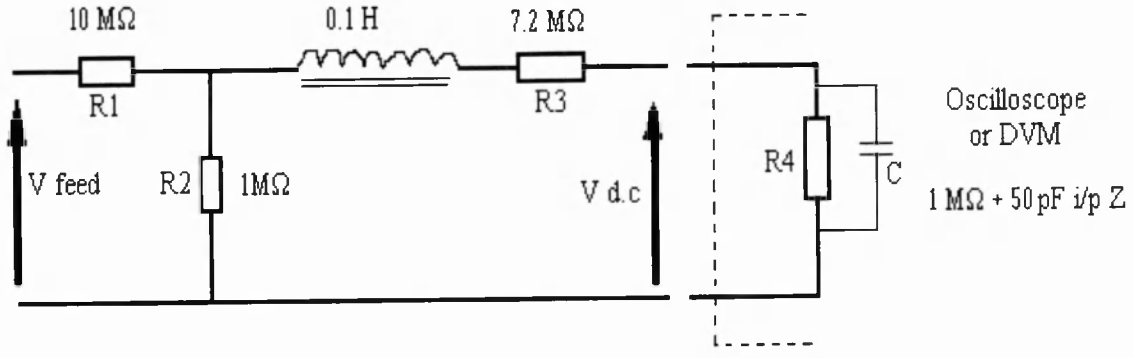

Figure 10. Circuit of the DC bias measurement.

The transfer function can be shown to be:

$$\frac{V_{dc}}{V_{feed}} = \left[\frac{Z_{meas}}{Z_{meas}+R_3+j\omega L}\right]\left[\frac{R_2(R_3+Z_{meas}+j\omega L)}{R_2(R_3+Z_{meas}+j\omega L)+R_1(R_2+R_3+Z_{meas}+j\omega L)}\right] \qquad \textbf{11}$$

Where Z_{meas} is the input impedance of the measuring device, in this case a digital volt meter and the coaxial cable feeding it (~ 50pF). $Z_{meas} = R_4 / (1 + j\omega CR_4)$. Figure 11 shows the attenuation as a function of $\log_{10}$ frequency.

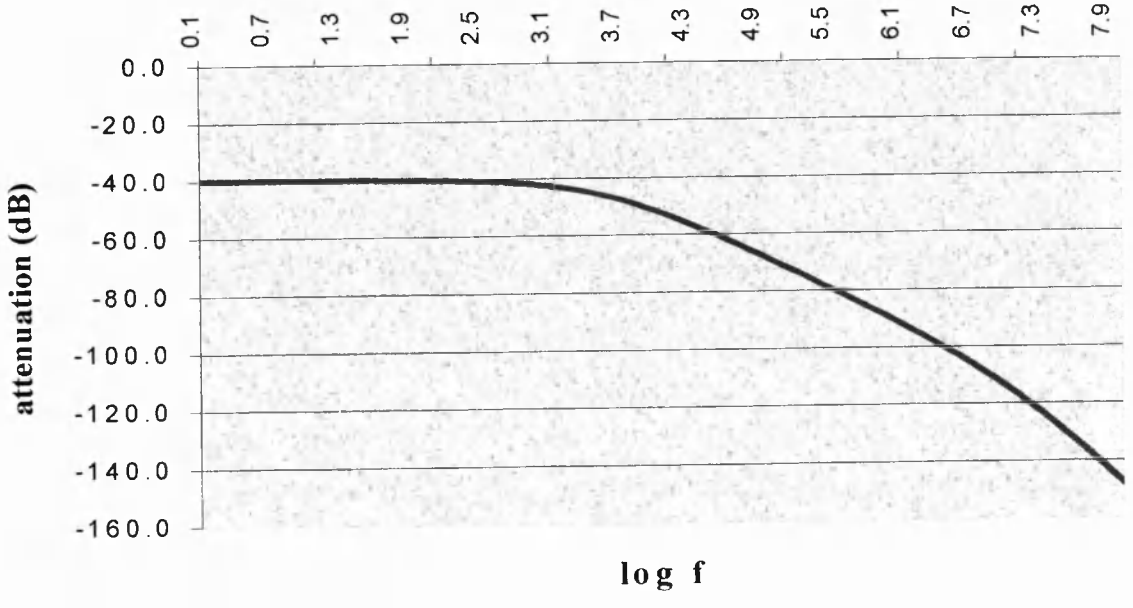

Figure 11. Frequency response of the DC bias probe.

It can then be seen from the response suggested in figure 11 that DC is attenuated by 40dB and the fundamental is attenuated by 117dB ($\log_{10}$ 13,560,000 = 7.13). In practice, the mean measured transfer function of the DC bias circuit at DC is:

V_{feed} / V_{dc} = **102.30** **(40.2 dB)** with a deviation of **0.00746**

At the fundamental frequency of 13.56MHz, the R.F. component at the output of the probe, V_{dc} is extremely small (not reliably measured) and considered suitable attenuation.

4. Experimental Considerations

4.1. Complete electrical model of the system

To get an understanding of the parameters we require and those easily obtained it is worth considering a representative model of the system.

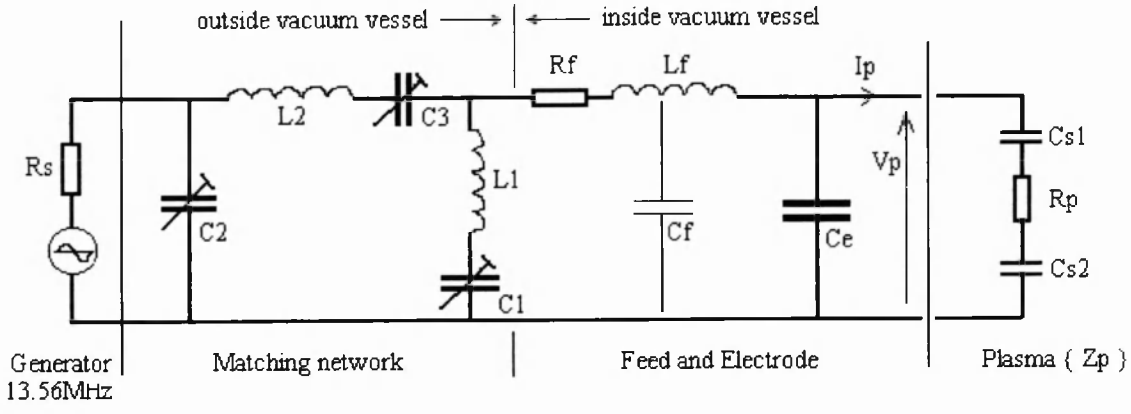

Figure 12. Electrical model of plasma feed system.

The generator has a source resistance, R_s of 50Ω. The matching network consists of two air cored inductors, $L_{1/2}$ and three variable air cored capacitors $C_{1/2/3}$. These components are all mounted in a single enclosure and the variable capacitors are adjusted for minimum reflected power seen back at the generator.

The vacuum chamber (or vessel) has a solid co-axial line from its external RF power connector to the driven electrode and this is termed the chamber feed. It can be represented by series resistance and inductance, R_f and L_f together with distributed capacitance to ground, in this case simplified to a lumped capacitance C_f. This feed is then shunted by a relatively large capacitance, C_e, due to the electrode and its earth shield, in parallel with the plasma impedance, Z_p (discussed in 6.2.1 as approximately $R_p + 1/j\omega C_{s1} + 1/j\omega C_{s2}$, plasma bulk resistance and sheath capacitances).

In addition to the power feed associated with structure inside the chamber, there is likely to be some form of coaxial cable prior to this from the matching network. The probe needs to be in series at some point of this line and ideally as close to the chamber as possible to minimise the amount of line that will need to be characterised (i.e. ideally prior to R_f).

4.2. Sensitivity considerations

The impedance of the plasma (Z_p) is to be determined from the externally measured voltage, current and through analysis of the network ($R_f + L_f + C_e$) in parallel with Z_p. The measured current includes both the true plasma current, I_p, and leakage currents caused by C_e and C_f. Plasma current will be mainly reactive (owing to the narrow space charge sheaths which dominate the impedance) and of small magnitude compared to the leakage current through C_e (and C_f). The effect of the electrode's capacitance, C_e on the accurate determination of I_p is therefore a considerable problem as a substantial current will flow (a reactive short) compared to plasma current which is smaller and can be quite close to 90° (in practice between 60° and 90°). Neglecting $R_f + L_f$, Z_p can be determined from the function:

$$Z_p = \frac{Z_m}{1 - j\omega C_e Z_m} \qquad 12$$

Figure 13 shows the plasma impedance Z_p, as derived from a measured impedance magnitude $|Z_m|$ (i.e. $|V_m| / |I_m|$) at a fixed value of measured phase, θ_m for C_e = 140pF.

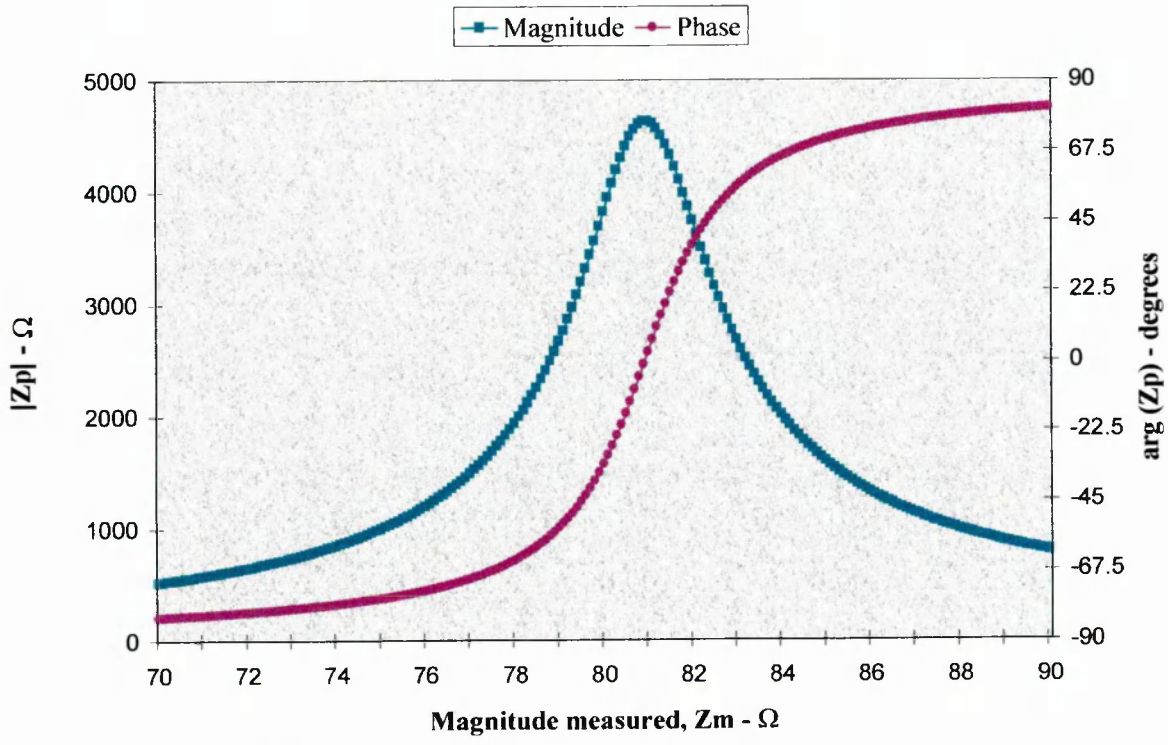

Figure 13. Magnitude and phase of plasma impedance (when shunted with electrode capacitance) vs. measured magnitude at an angle of -89°.

It is noted that at measured phase angles approaching -90° the value of Z_p changes at large rates about its phase change.

To represent the sensitivity of Z_p to variations in both the magnitude and angle of a measured Z_m, contour plots in the complex plane are illustrated in figures 14 and 15.

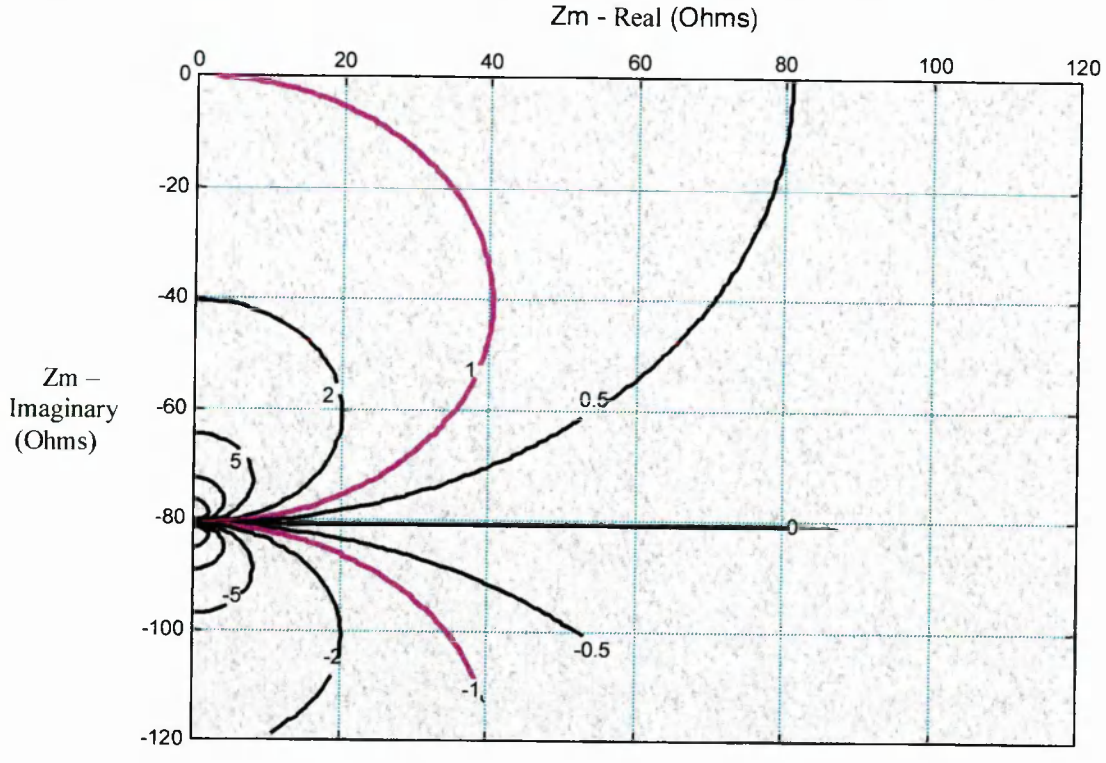

Figure 14. Magnitude sensitivity contours of $|Z_p|$ as a function of Z_m due to electrode capacitance.

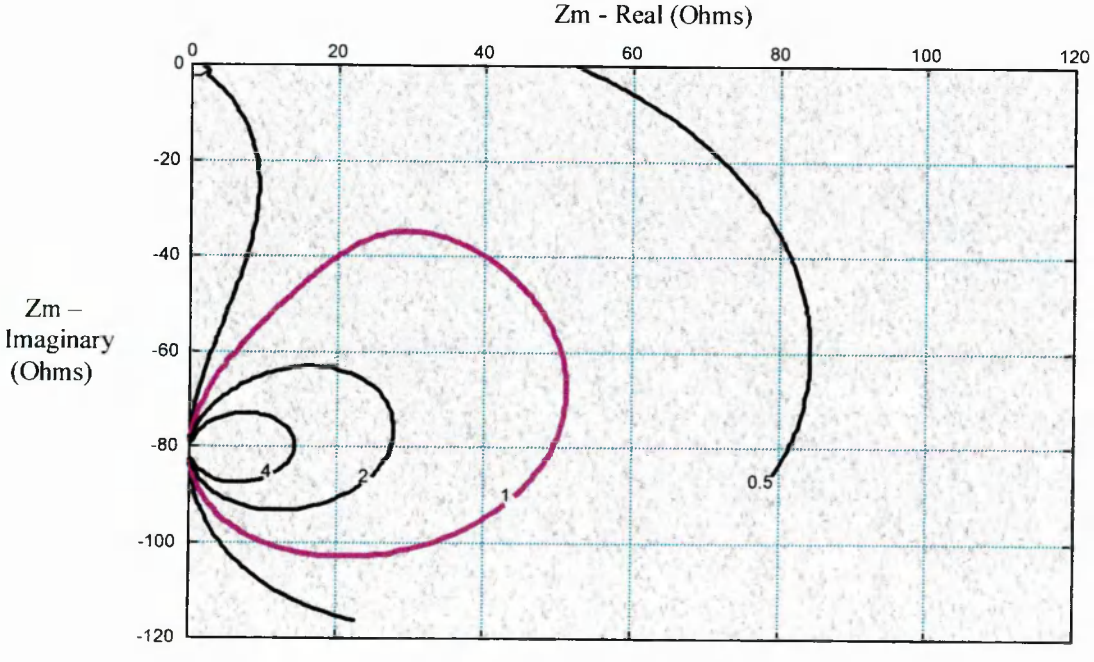

Figure 15. Phase sensitivity contours of $|\theta_p|$ as a function of Z_m due to electrode capacitance.

These contours are therefore gradients which relate the error of the measured parameter against the corresponding error that will arise in Z_p, when determined from equation 12.

The magnitude sensitivity contours represent the ratio of *fractional* change in $|Z_p|$ to that in Z_m. The contour values are given by:

$$\frac{\partial|Z_p|}{\partial|Z_m|}\frac{|Z_m|}{|Z_p|}$$

The phase sensitivity contours represent the ratio of *absolute* change in $|\theta_p|$ to that in Z_m i.e. degrees per ohm, and are calculated from:

$$\frac{\partial|\theta_p|}{\partial|Z_m|}$$

Regions with gradients of less than 1 on these plots actually result in de-sensitising our measurements, however, the majority of this complex region (likely in practice to be typical) results in high/extreme sensitivity.

The scale of the sensitivity problem can now be seen, especially when attempting to evaluate Z_p from a measured Z_m near 80Ω ($=1/\omega C_e$) at angles approaching -90°. The only practical solution (without developing methods of unreasonable precision) is to null the effect of this capacitance with a shunt inductance.

4.3 Shunt tuning and placement of the VI probe

Ideally the current that flows in C_e needs to be cancelled out of the system. This can be achieved by placement of an inductor of the same impedance in parallel with the capacitance, forming an equal loop current due to the opposite phase of these currents.

The matching network consists of C_2, L_1+C_1, and L_2+C_3 in a π-shaped network of which the final L_1+C_1 can be used to counteract the impedance of C_e. Placement of the probe would then be between C_3 and the L_1+C_1 series network. C_1 should then be tuned for minimum measured current without vacuum present in the plasma chamber (i.e. R_p is infinite and C_p is zero).

In this case, C_1 (and hence shunt impedance) will not cancel Z_{Ce} completely because of the series loss and inductance component in the coaxial and chamber feed. With typical power levels (50-100W) this can relate to leakage currents of the order $50mA_{rms}$. This can only be reduced by employing a dedicated shunt (leaving L_1+C_1 purely for matching purposes) directly under the chamber to reduce loss in the loop.

The probe can now be placed ahead of this shunt inductance. The loop current will now minimise the leakage current seen to ground but it will still not reduce it to zero because of the residual loss (and series inductance) incurred from the minimal amount of chamber feed present.

Effectively this leakage current can then be accounted for as a parallel component that replaces C_e (and shunt) and will have an impedance that is complex, shown as $R + jX$ in figure 16.

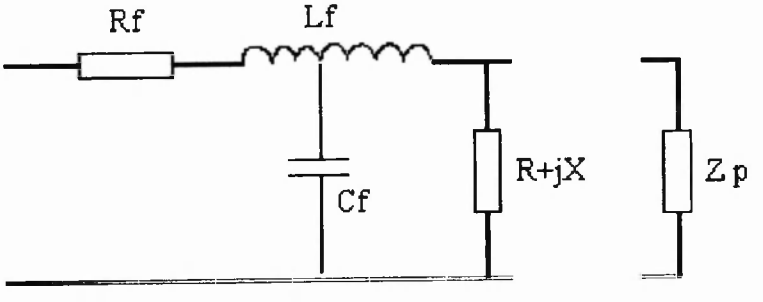

Figure 16. Model of feed when electrode capacitance partially nulled with shunt inductance.

The current into an empty chamber (through $R + jX$) is reduced to a few mA, the measured impedance of the chamber being calculated at 6960Ω with a small angle of +1.4°. This is quite a high impedance (compared to those typical of plasmas) and nearly entirely real, suggesting that any effort to compensate for this current may not be as valuable as first thought.

Sensitivity contours are now shifted in the complex plane so that the points of high gradient are now at approximately 7kΩ and on the real axis, as shown in figure 17. Typical measurements will now be far from this region of impedance and therefore the network is effectively de-sensitised.

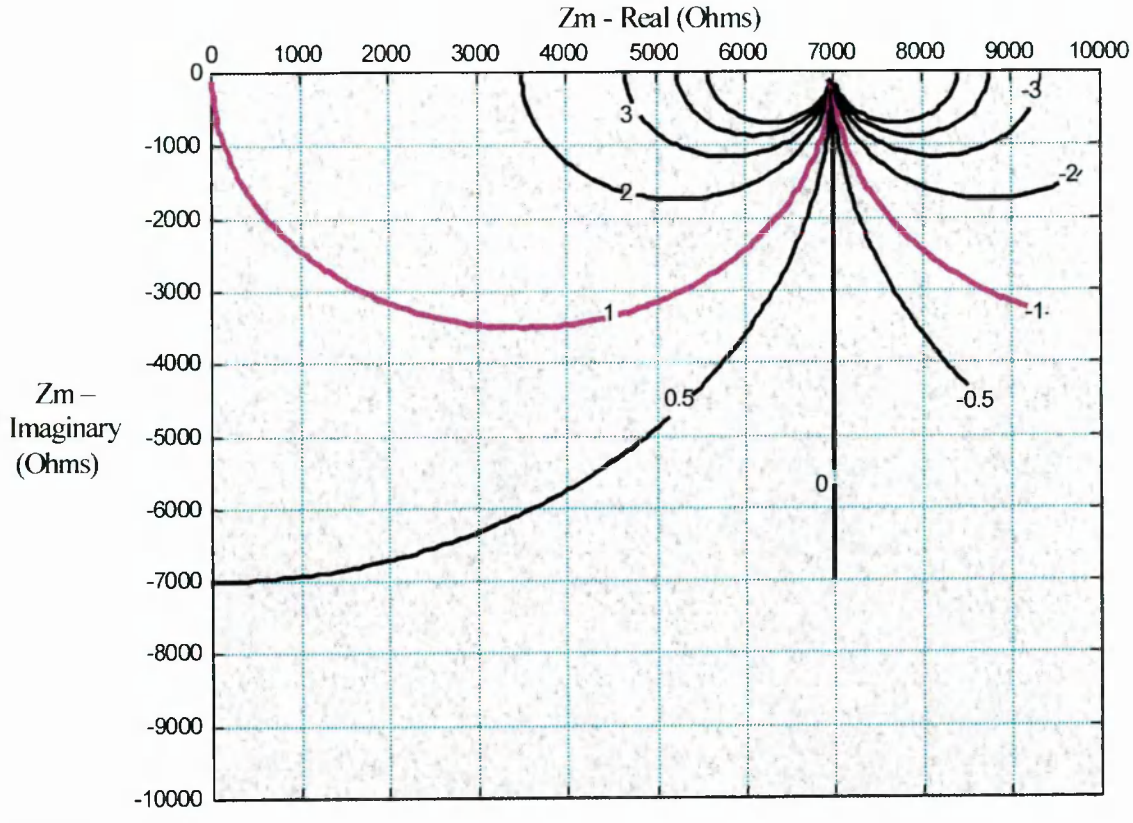

Figure 17. Sensitivity contours of $|Z_p|$ as a function of Z_m when electrode capacitance is partially nulled by shunt inductance.

4.4. Feed Characterisation

Characterising any two port linear network such as a transmission line can be approached from either of two ways. The simplest method is to treat the network as consisting of lumped elements as previously discussed, whilst a more complete method, especially at this frequency, is to consider the network as containing distributed elements. Whereas a simple model will have a single R, L and C in parallel, distributed components would suggest R/n, L/n and C/n, per part of n sections. Voltage and current components together with impedance calculations are determined using a transmission line model as shown in appendix D.

Initially however, estimations have been made for the various components in the original model, RLC.

4.4.1. Electrode Capacitance

In the system tested, the driven electrode is a metal disc of approximately 94mm diameter by 12mm depth with a grounded shield on the underside. Estimating capacitance from the dimensions measured suggests a capacitance of about 100pF. This value was then compared to a measurement (at DC) from a digital meter which suggested 92pF. This latter figure is likely to be more accurate but will consist of not only the electrode's capacitance but also that of the chamber's co-axial line, C_f (section 4.4.2). Essentially this is of little concern to us as current due to this is cancelled by the shunt.

Electrode capacitance is however useful to know as it can be used as a calibration parameter to complete a simple transmission line model.

4.4.2. Feed Capacitance

Feed capacitance, C_f was estimated from a DC capacitance measurement of the chamber feed without the electrode attached. An approximate value of 30pF +/- 3pF was obtained using a digital meter

Section 4.5 of this report discusses the benefits of a distributed over a lumped model, as well as equating the two models together in order to confirm the initial measurement of C_f.

4.4.3. Feed Loss

If we test for the power into the chamber system with no vacuum present (i.e. a plasma cannot be excited) the resistance of the feed can be estimated. The test arrangement consisted of the generator feeding the chamber feed via the VI probe and a 1/2 metre cable between probe and chamber.

$$Power = VI\cos\theta = I^2R$$

Therefore

$$R = (V\cos\theta)/I$$

[where V and I are rms values.]

Power on the generator was set to 9.8W and the generator indicated a reflected power of 7.5W. The probe indicated a power of 1.46 watts and a current of 0.606 amp leading voltage by 85.9°. This indicates a resistance of about 4Ω which would appear to be quite high. Considering the cable's dimensions, the length of the co-axial feed within the chamber and the effects of skin depth, a more realistic value should be in the region of 1Ω.

It should also be noted that a real transmission line will have dielectric loss as well as series conductor resistance, but this is not considered in a simple model.

4.4.4. Feed Inductance

The feed inductance can be estimated from knowing C (C_{feed} + C_e) and the resonant frequency. The system's feed is an RLC series circuit where the impedance seen into the chamber (without the shunt and vacuum) is:

$$Z = R + j(\omega L - \frac{1}{\omega C}) \qquad \textbf{13}$$

At resonance: $\omega L = 1/\omega C$ and $Z = R$, therefore: $L = 1/\omega^2 C$

Resonant frequency is the frequency at which a peak in the measured current is observed. For this particular arrangement resonance occurs at 31.2MHz +/- 0.2MHz.

For C=92pF and Freq.= 31.2MHz, L is estimated as 282nH +/- 3nH

At resonance $Z = R$ and hence this is an additional method of determining R from the V and I measured. To do this the probe would need to be calibrated at the resonant frequency (31.2MHz) in the same way as calibrating at 13.56MHz.

4.5. Comparison against Distributed TX Line Model

Characterise entire feed system

This is a calibration procedure decided upon from work inspired during a visit to Queens University, Belfast and is a method of treating the entire feed system as a TX line. This involves determining the characteristics of the probe and the characteristic impedance of the connection to the plasma electrode, as though it were one transmission line. The connection system includes a standard N-type co-axial connector and the co-axial line prior to the electrode (within the chamber). This chamber feed comprises series inductance, series loss, distributed capacitance and dielectric loss. Transmission line principles (outlined in appendix D) allow a full model of the connection system to be analysed.

Procedure

Impedance of the chamber system alone is measured by the probe for two distinct conditions. Firstly an open circuit impedance, $Z_{o/c}$ is determined. This is the impedance measured by the probe of the entire connection system, with the shunt and electrode in place, when no load is being presented (i.e. an unevacuated chamber therefore plasma is not excited). This is mentioned in section 4.3 and calculated as $Z_{o/c} = 6960 + j.170$ ohms. Secondly, a short circuit impedance, $Z_{s/c}$, is measured. In this case the electrode is replaced by a mechanical short circuit cap (see figure 6) and the shunt inductance is removed, as it is only used to form a loop current with the electrode capacitance.

The characteristic impedance, Z_0 and γl (propagation constant x length) of the entire transmission line can then be determined from equations D4, 5. Once these parameters are known equations D1, 2 and 3 can be used to determine V_{load}, I_{load} and hence Z_{load} in the routine IV_COMP.XLS.

Equating the two models

The measurement of $Z_{s/c}$ can be equated with the real and imaginary series components of the feed, to obtain lumped elements R_f and L_f.

$$Z_{s/c} = R_f + j\omega L_f = 0.33 + 6.6\,j$$

From this we can deduce that $R_f = 0.33\Omega$ $L_f = 6.6/\omega = 77\text{nH}$

The open circuit measurement, $Z_{o/c}$ can only be related to the RLC model when the shunt and electrode impedances are included.

C_f and C_e need to be estimated in order to determine the shunt impedance (of the inductor) that will give a measured $Z_{o/c}$. This shunt impedance can be considered an inductance with some loss, $R_{sh} + j\omega L_{sh}$ and is easily analysed in the model.

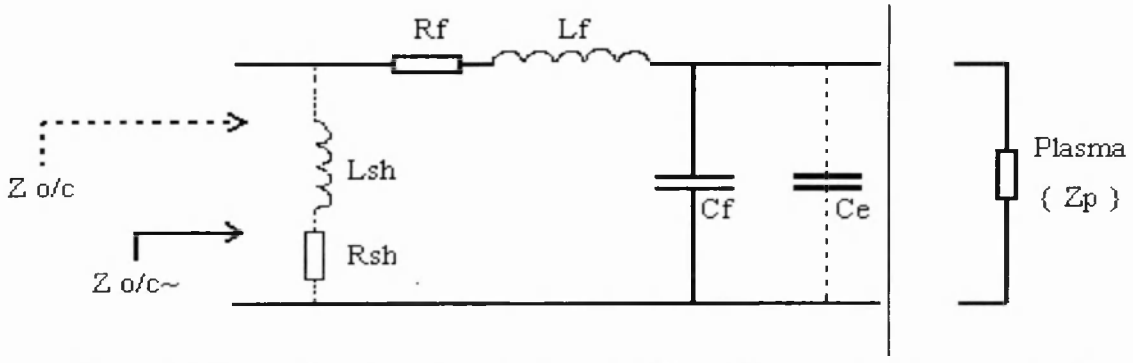

Figure 18. Lumped model of the chamber feed including shunt capacitance and inductance.

An estimate of feed capacitance, C_f can be made from an open circuit measurement, $Z_{o/c\sim}$ of the feed when no electrode and shunt are connected

$$Z_{o/c\sim} = R_f + j\omega L_f - j\left(\frac{1}{\omega C_f}\right) = 10 - 415\ j$$

It is not possible to equate these measured impedances with expressions for this model due to the inherent differences but it can be approximated. Neglecting the real part of the open circuit impedance gives:

$$C_f = 1/(\omega\ 422) = 28\text{pF}$$

C_e was measured with a digital capacitance meter as 92pF.

Using a maths package, R_{sh} and L_{sh} are determined as 0.864Ω and 1.07uH given $Z_{o/c}$, R_f, L_f, C_f and C_e as above. Plasma impedance, Z_p can then be determined given a particular measured impedance of the network, Z_m.

By equating these measurements to obtain this simple model, a comparison can be made between lumped and distributed models for typical plasma measurements. This will then give an indication of the size of error inherent to simple lumped networks.

The error that occurs through the approximation to this model is included in the main analysis routine IV_COMP.XLS for interest. Errors are not massive, but error in phase of a few degrees is significant when measuring power in a highly capacitive plasma load, as explained earlier.

5.Software Analysis

The data from the VI probe is displayed on a LeCroy oscilloscope (300MHz Digital storage oscilloscope) and analysed in software to take account of the VI probe's transfer functions and any subsequent processing such as Fourier analysis. All programming is performed in Microsoft EXCEL for ease of use and graphical representation. The analysis program is called IVPROBE.XLS. At present it consists of the Fourier analysis routine (IV_FA.XLS) and the feed transfer function routine (FEED_TF.XLS).

At a later date it is intended to incorporate, and hence account for, error propagation (IV_ERROR.XLS). A more complete routine has been assembled (IV_COMP.XLS) that is derived from IVPROBE.XLS but only analysing up to the third harmonic and taking account of the TX line between probe and chamber (feed system and load). See appendix D.

5.1. Fourier analysis of measured waveforms

The plasma is a very non-linear load and hence Fourier analysis allows us to extract the phase and amplitude of the fundamental voltage and current waveforms. At the same time we can analyse the second harmonics and above. Any periodic waveform can be represented as the sum of an infinite number of sine and cosine harmonics.

$$f(t) = a_0 + \sum_{n=1}^{\infty} a_n \cos(n\omega t) + \sum_{n=1}^{\infty} b_n \sin(n\omega t) \qquad \textbf{14}$$

where a_0 is the dc offset. To determine these components (n=1, 2, 3 etc.) we integrate the function, weighted by the harmonic, over one period:

$$a_n = \frac{1}{T}\int_0^T f(t)\cos(n\omega t)dt \qquad \textbf{15}$$

$$b_n = \frac{1}{T}\int_0^T f(t)\sin(n\omega t)dt \qquad \textbf{16}$$

T is the period of the fundamental.

The magnitude of the first or subsequent harmonics is now:-

$$|A_n| = \sqrt{a_n^2 + b_n^2} \qquad \textbf{17}$$

and the angle is determined from:-

$$\Theta_n = -\arctan\left(\frac{b_n}{a_n}\right) \qquad \textbf{18}$$

The software calculates, at the fundamental and each harmonic frequency, the phase of the voltage and current data to determine the amount of current lead in each case before being passed onto the routine dealing with the TX line and transfer function of the feed.

The Fourier analysis routine is very large, mainly because it works out amplitude/phase for components up to the seventh harmonic. This is not entirely necessary as distortion in these waveforms is observed as being mainly (and strongly) second and third harmonic.

5.2. Layout of the Power & Impedance analysis spreadsheet

Placement of the probe and considerations with respect to the shunt and transmission line calibration has been discussed. It is now necessary to tie this all together into the analysis routine. Figure 19 shows a demonstrative example of this spreadsheet.

The spreadsheet is given calibration parameters, namely the transfer function of the probe at the fundamental (and approximations for its behaviour at the second and third harmonic determined from the modelling in section 3.1 which suggested that the probe is differential at frequencies up to those of interest). The other calibration parameters required are open and short circuit impedance measurements together with frequency of the fundamental and an estimate of wave propagation velocity in the line.

Various characteristics of the transmission line are given in the spreadsheet for interest such as Z_0, α, β (attenuation and phase coefficient, appendix D) and the transmission line's 'effective' length. The last three are dependent upon an estimate of propagation velocity. The dielectric in the chamber feed is Teflon ($\varepsilon_r \approx 2.1$) and therefore propagation velocity will be $\approx 2 \times 10^8$ m s^{-1} (velocity of propagation in air, 3×10^8 m s^{-1} divided by the square root of 2.1).

Measured signal parameters are determined from the Fourier analysis of the waveforms measured and the probe's transfer functions. These values are then considered to be the voltage and current on and through the line at the point of measurement. There are obviously two points of measurement, one for voltage and one for current but the calibration procedure outlined in section 4.5 & appendix D takes account of this when determining V and I at the electrode.

The routine then works out the plasma characteristics using the transmission line model (equations D1, 2, 3, 4 & 5). At the same time calibration parameters are equated to a RLC lumped model equivalent circuit to show the size of errors that would have occurred through use of the simpler model.

In summary, the complete routine (VI_COMP.XLS) determines the following.

* ***V, I, & Current lead*** at the entrance to the feed (determined in, and passed from, the Fourier analysis routine).
* ***V, I, & Current lead*** at the driven electrode.
* ***Plasma Impedance*** in Cartesian form.
* ***Resistance*** and ***Capacitance*** of the Plasma.
* ***Plasma Power & Feed Efficiency.***
* ***Harmonic Distortion*** for V and I up to the third order.
* ***Plasma Impedance*** from the lumped model.

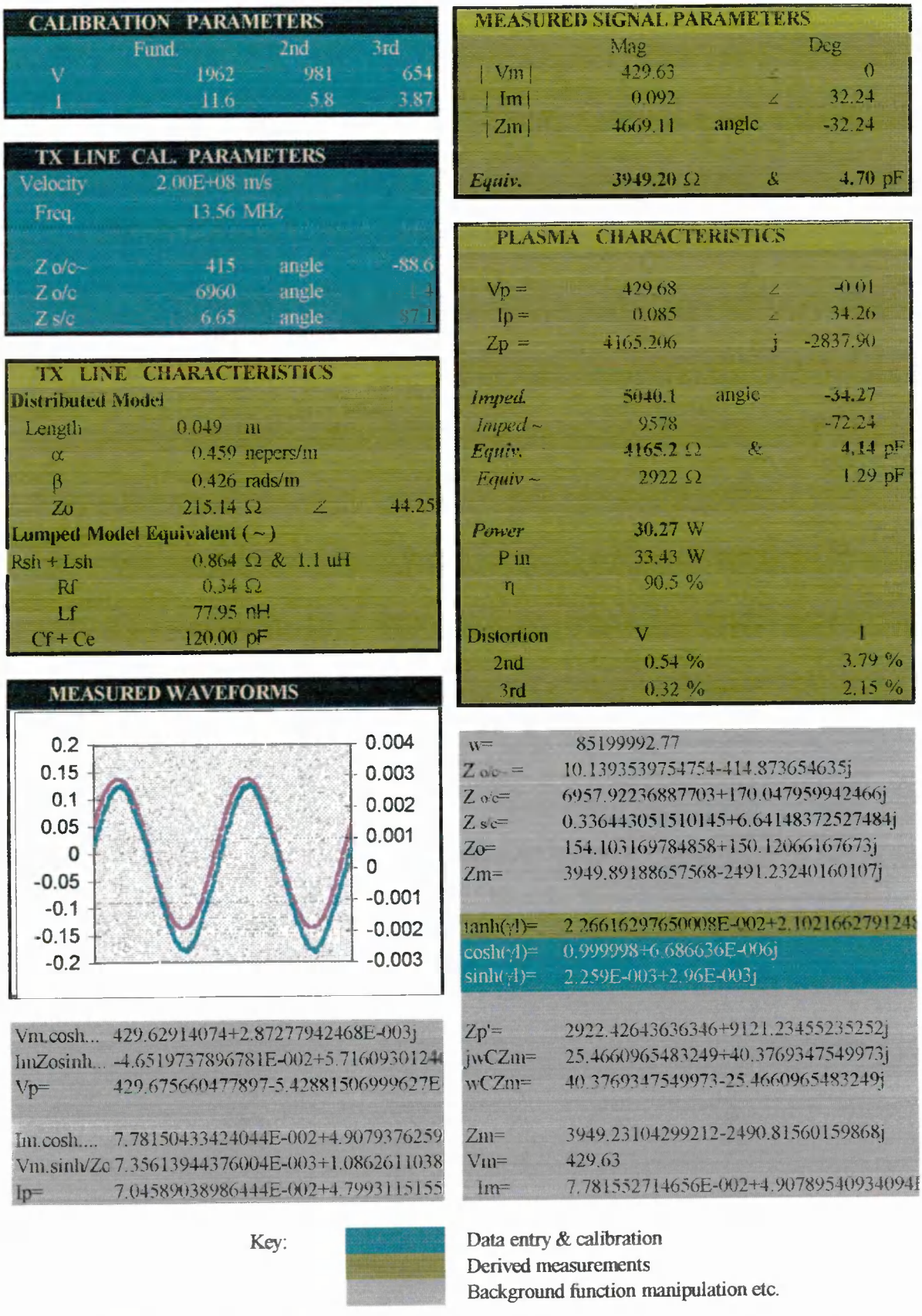

Figure 19. Example spreadsheet of the Power & Impedance analysis routine.

It should be noted that Excel 5.0 is not capable of performing complex inverse hyperbolic trig functions so cosh γl and sinh γl need to be determined from the calculated tanh γl with a separate maths package. This is not considered a problem as they remain constant for a particular TX line and hence system.

6. Measurement Examples

6.1. Complex Test Loads

Several different types of complex loads were constructed to evaluate the VI probe and software by comparison with expected results.

Impedances were made with microwave quality capacitors of various values and tolerances whilst resistance was either a 50Ω termination (as in the calibration) or two of these in parallel to make 25Ω. In a similar manner to the 50Ω calibration load these were then mounted on the end of an 8cm microstrip launch (transmission line) and attached to the probe via an N-type connector.

The following list gives expected values (see appendix B) for a network together with measured impedances from both Mk1 and Mk2 probe designs.

The reason for the development of the Mk2 probe was to eliminate loading due to the significant coupling apparent with the Mk1 design. It was observed that the error in the measured parameter seemed to be related to the magnitude of impedance and the design of this probe is very similar to that of Mk1 but with some minor changes. These are highlighted in appendix C together with designs MK3/4.

No.	Network type	Expected Z	Mk1 Z	Mk2 Z
1	470pF//25Ω	17.7 @-45°	13.6 @-21.1°	15.2 @-37.9°
2	470pF+25Ω	35.3 @-45°	29.3 @-37.4°	31.6 @-42.6°
3	100pF//25Ω	24.5 @-12.0°	23.7 @+3.7°	23.4 @- 6.4°
4	100pF+25Ω	120 @-78.0°	83.6 @-79.4°	98.7 @-79.1°
5	470pF	24.97 @-90°	18.2 @-89.1°	20.8 @-89.3°
6	100pF	117.4 @-90°	81.0 @-88.0°	100.5 @-89.9°
7	50Ω	50.5 @-0°	53.4 @-0.6°	50.97 @-0.3°

Table 1. Probe measurement performance into complex loads.

Note: '//' represents a parallel network.
'+' represents a series network.

These results show a clear improvement in accuracy from the Mk2 design over the original. In some cases the error on Mk2 designs is on the border of the components' tolerance but is generally more realistic than Mk1 results.

Incorporation of TX line model.

As described in appendix D a transmission line model is required to determine load impedance from measured impedance. The results from applying this model to the above measurements are extremely encouraging.

No.	Expected Z	Mk2 & TX model	Mk2 Z	Mk1 Z
1	17.7 @-45°	16.8 @ -43.5°	15.2@-37.9°	13.6@-21.1°
2	35.3 @-45°	33.8 @ -44.3°	31.6@-42.6°	29.3@-37.4°
3	24.5 @-12°	23.8 @ -10.6°	23.4@ -6.4°	23.7@ +3.7°
4	120 @-78°	111 @ -78.3°	98.7@-79.1°	83.6@-79.4°
5	25.0 @-90°	23.5 @ -89.4°	20.8@-89.3°	18.2@-89.1°
6	117.4 @-90°	113 @ -89.9°	100 @-89.9°	81.0@-88.0°

Table 2. Measurement performance with and without inclusion of the TX line model.

The TX line model takes into account velocity of propagation along the line 'v' as being 1.5×10^8 m s^{-1} (glass fibre board $\varepsilon_r \approx 4.5$), length of line to be 8cm and characteristic impedance to be 50Ω. These values have not been accurately measured, but for initial analysis they enable us to confirm and validate the direction of this work.

Figure 20 is a graphical representation of these results and shows good contrast between performance of both designs as well as the effect of incorporating the TX line model.

It is interesting to note, in the case of 100pF and 25Ω networks (3 and 4), that the estimated component values in the series and parallel networks are converging on expected values. The Mk2 design alone suggests component values to be 18.7Ω + 121pF and 23.5Ω // 56pF (for the series and parallel networks respectively) whilst inclusion of the model suggests 22.5Ω + 108pF and 24.2Ω // 91pF . There is an obvious convergence to the indicated 100pF capacitor and although dependent on the parameters of the TX line model it also tends to the suggested value of capacitance from network #6 (100pF capacitor alone) of $C = 1 / 2\pi f|Z| = 103.9$pF.

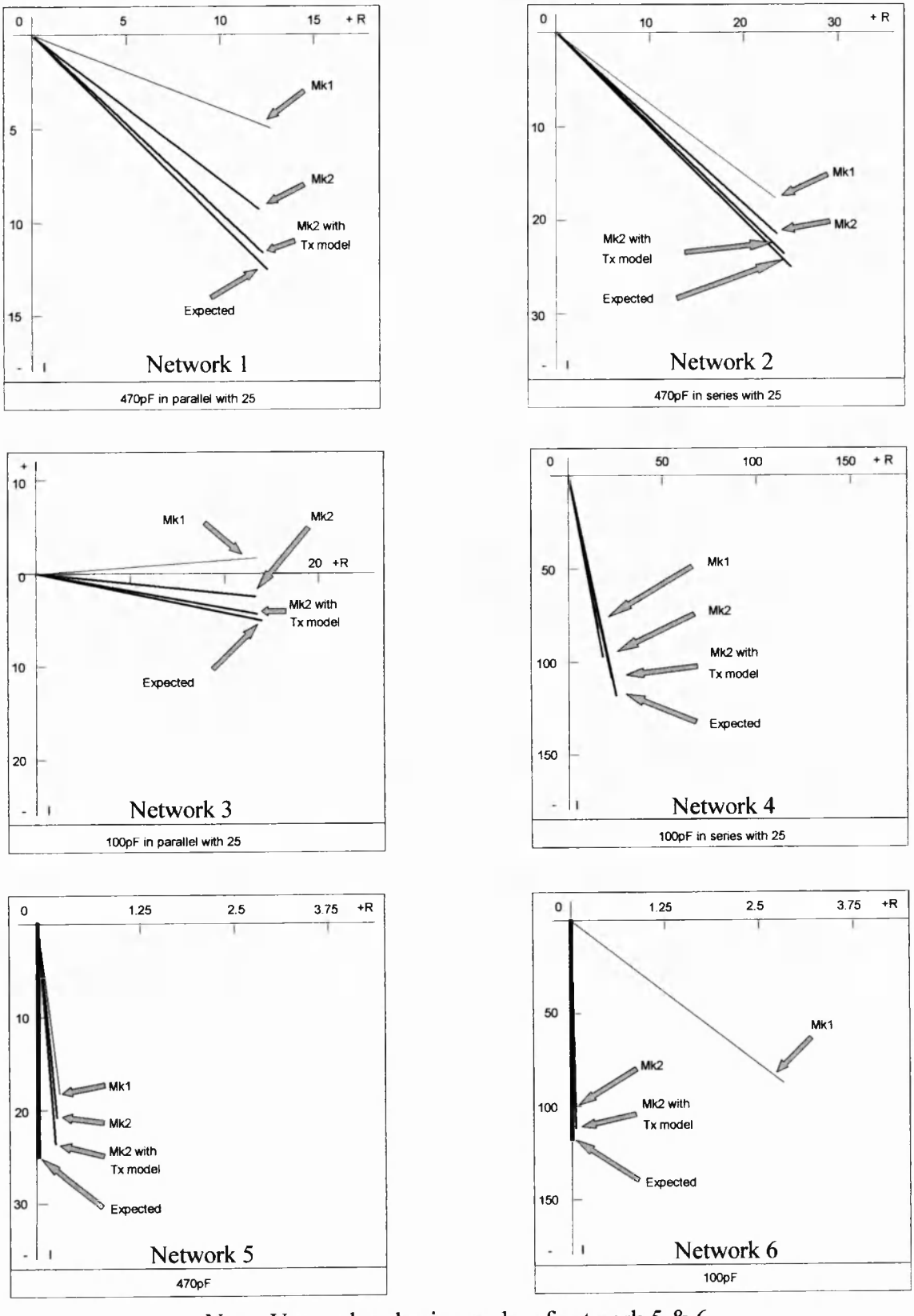

Note: Unequal scales in graphs of network 5 & 6.

Figure 20. Graphical comparison of measurement performance.

6.2. Plasma Discharge

The majority of experiments performed during this research concerned measurements on the 'typical' plasma (i.e. capacitively coupled, argon gas at 10-100Pa and excited by a 13.56MHz source). They consisted of two different analysis procedures, initially not accounting for the transmission line model and towards the end of the work in realising its inherent necessity.

6.2.1. Initial Analysis

Impedance measurements are an invaluable diagnostic tool for use in both industry as well as research. An experiment has shown the effect that electron injection (into the bulk of a 50mtorr argon plasma) has on Langmuir probe measurements[4]. This is an electrostatic probe that can be used to determine the flux of various species within the plasma bulk. These measurements taken in conjunction with those of impedance allow further understanding of the interaction between physical and electrical mechanisms.

The VI probe was connected ahead of a shunt inductance and then via coaxial cable to the chamber during this experiment, the voltage and current waveforms were analysed and expressed in various forms as a function of injection electron current.

The results are presented in figure 21 and although the analysis takes account of the TX line feed as an RLC lumped circuit and does not include the shunt, the measurements show consistent relationships.

A plasma can be represented by a crude model that consists of two capacitances (from the ground and driven electrode sheath) and a resistive component (the bulk of the plasma) in series i.e.

$$Z_{plasma} = 1/\jmath wC_{sheath1} + R_{bulk} + 1/\jmath wC_{sheath2} \qquad \textbf{19}$$

In turn this can be represented as a resistance and single capacitance in series. These parameters, deduced from the V and I waveforms, are related to various physical mechanisms occurring in the plasma (a more thorough model is presented in section 6.2.2).

Capacitance

As mentioned, capacitance is a function of the sheath dimensions which in turn are a function of the plasma potential. As electrons are injected into the bulk, the dc potential across the sheath will drop and in general the sheath will become narrower. The sheath on the grounded electrode in this case is the chamber walls and hence the larger area will lead to more capacitance. However, the smaller capacitance from the driven electrode will dominate the total capacitive reactance in this situation.

The driven electrode is 10cm in diameter and 1cm thickness. With a sheath thickness of about 5mm this relates to a sheath capacitance of the order of 15pF. This is clearly below that measured and it is probable that the simple feed model used is the cause of this. However measured capacitance is increasing with electron current as theory would suggest.

Resistance

Resistance is mainly determined by plasma conductivity although various other dissipation mechanisms will contribute. An increase in plasma density will cause an increase in conductivity (due to more species being available for conduction) and hence a reduction in resistance. Density is a function of pressure and temperature and therefore a pressure increase or temperature decrease will cause a similar effect on bulk resistance as will increasing electron density as in this case. From the graph it is apparent that resistance decreases with electron gun input current tailing of after about 400mA. This is similar to the capacitance measurement and would suggest that the gun's electron output is saturating at this level of input current. The parameter 'injected electron current' is the measured current consumption of the gun as opposed to the real emission current and it is apparent that they are not linearly related.

Phase Angle

The phase angle is derived directly from the V and I waveforms and is therefore another parameter that can be used for diagnostics etc. Again this graph indicates some saturation in its upper region and the measured change in phase is substantial for the change in bulk density. The initial value of about 67° would seem to compare well with observations made by M. Sobolewski in similar geometry chambers [5].

Plasma Power

The RF generator for this experiment was set to 25W forward power and after the shunt inductance was tuned under vacuum conditions, the matching network was adjusted for zero reflected power. Previously it has been observed that the generator displays approximate power (normally about 90% of the output power) and so it is of little concern that power measured in this case slightly exceeds 25W. The power in the plasma decreases with injected electron current but this is due to the matching network being set only at the initial run of the experiment. At 400mA electron current the plasma has a significantly different impedance to that with 0mA and hence will need to be matched at each measurement point. The output metering of the RF generator is not accurate and can only be used as a rough indicator.

Distortion

Distortion is merely an observation at present and in due course it is hoped to relate this to various mechanisms associated with the increase in bulk density.

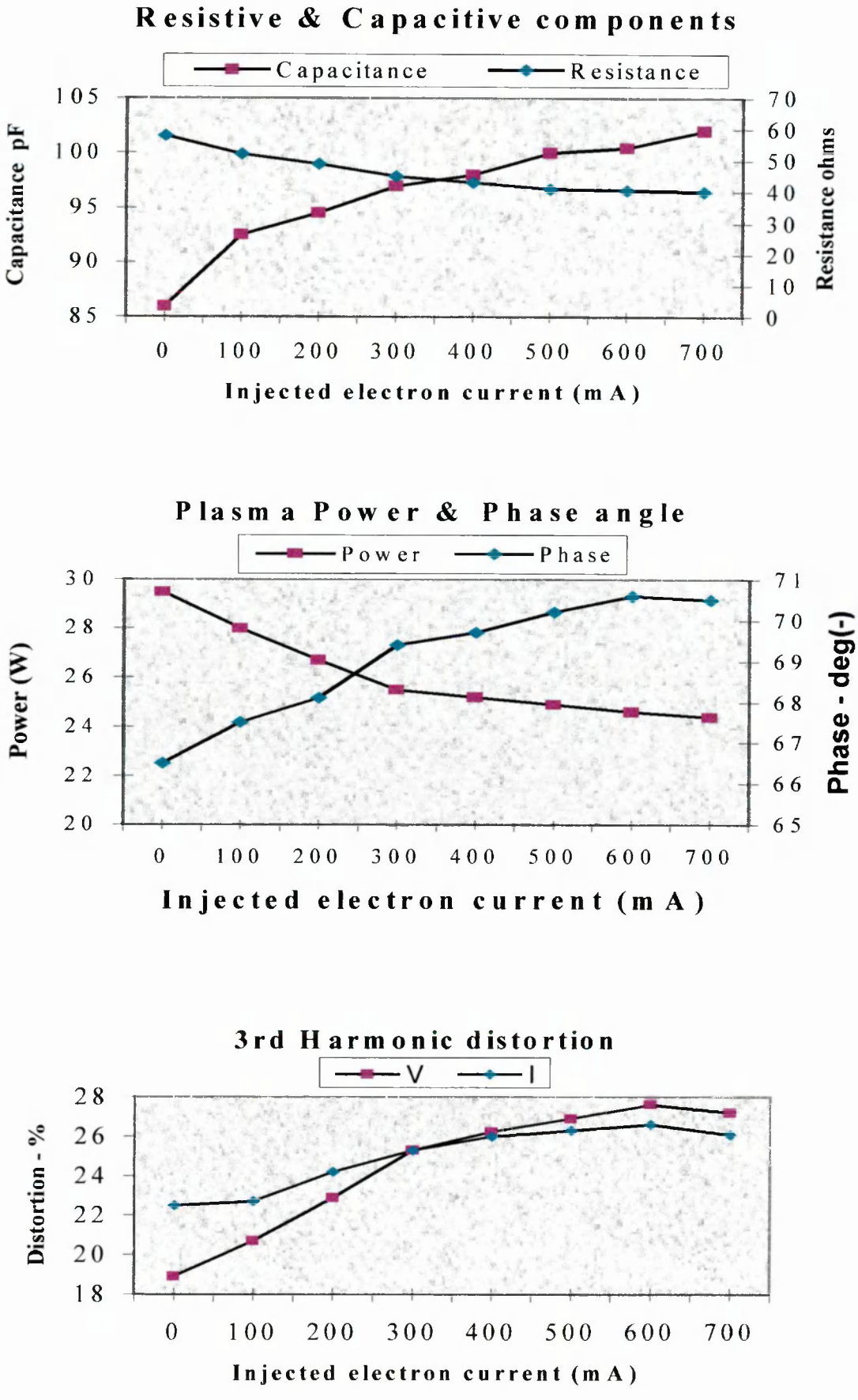

Figure 21. Impedance, power & distortion as a function of injected electron current.

6.2.2. Further Analysis

The inclusion of a transmission line model, an accurate calibration of the feed and probe together with earlier decisions on placement and shunt tuning etc. would lead us to believe that any impedance on the electrode is now measurable with a fair degree of confidence.

However, analysis of the plasma at a higher depth of modelling is needed to confirm the initial belief of this type of plasma exhibiting predominantly capacitive impedance.

The plasma is generated within a parallel plate chamber geometry and the impedance measured is that of the plasma *and* components introduced by the chamber. In the type of system used there is a driven electrode at the bottom of the vacuum chamber with the chamber and the top electrode being grounded. This ground electrode is attached to the top of the cell with a thick metallic rod. Some inductance and series loss will obviously be induced here but they will be extremely small and can be considered negligible.

Figure 22 shows a model of the components within the plasma's sheath and bulk to determine whether the plasma impedance will be predominantly capacitive or inductive.

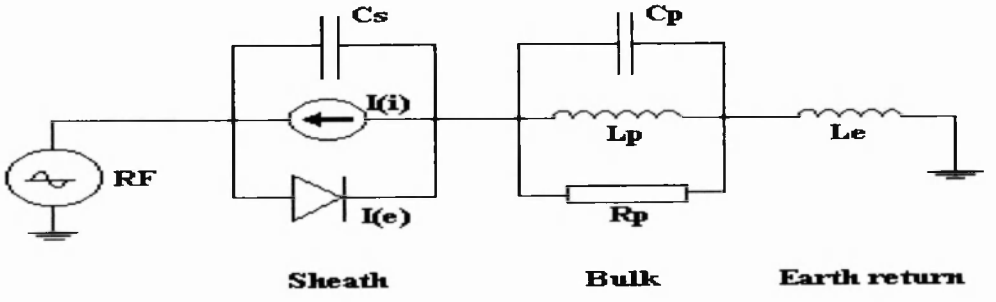

Figure 22. Plasma sheath and bulk model.

In this model there are two resonant conditions possible. Either a parallel resonance between L_p and C_p or a series resonance between L_p and C_s . If we consider each combination by relating the electrical to physical parameters, a physical situation can be proposed in which the plasma will behave with dominant capacitance.

Note the inclusion of ion current flow, *I(i)* and electron current flow, *I(e)*. These mechanisms will not affect impedance measurements but will be a cause of non-linearity.

C_p L_p parallel resonance

The plasma bulk's resonant frequency ($\omega_{p(e)}$) is determined by electron inertia (L_p) and vacuum displacement capacitance ($C_p = \varepsilon_0 A / d_p$) where ε_0 = free space permittivity, A= effective cross sectional area and d_p is the bulk's depth or length.:

$$\omega_{p(e)}^{2} = \frac{1}{C_p L_p} = \frac{n_e e^2}{m_e \varepsilon_0} \quad [6] \qquad \textbf{20}$$

This natural resonant frequency of the bulk's electrons is dependent on electron density, charge, mass and permittivity. For typical values, the resonant electron frequency is of the order 250MHz and therefore the bulk will behave *inductively* when excited by 13.56MHz as used in this system.

C_s L_p series resonance

Resonance between sheath capacitance and bulk inductance occurs when ω_{rf} is equal to ω_{res} where:

$$\omega_{res}^{2} = \frac{1}{C_s L_p} \qquad \textbf{21}$$

If $\omega_{rf} < \omega_{res}$ then plasma impedance will be capacitive. Therefore the following will need to hold true:

$$\omega_{rf}^{2} < \frac{1}{C_s L_p} \qquad \textbf{22}$$

Rearranging equation 20 and substitution into equation 22 gives:

$$\frac{\omega_{rf}^{2}}{\omega_{p(e)}^{2}} < \frac{C_p}{C_s} \qquad \textbf{23}$$

Capacitance is inversely related to depth, d, so using the estimate of $\omega_{p(e)}$ gives:

$$\frac{13.56\,MHz}{250\,MHz} < \sqrt{\frac{d_s}{d_p}} \qquad \textbf{24}$$

The plasma's impedance will be predominantly capacitive when the bulk length is less than about 400 times the sheath length. An estimate of sheath length is therefore needed.

Sheath length (i.e. the distance across the space charge region between electrode and plasma bulk) is a dynamically satisfied parameter within the system which settles to a steady state condition within microseconds of the exciting RF power being applied. As a general rule it is of the order of ten times the Debye length. This is a measure of the distance, within the bulk, over which the electric field of an individual charged particle will influence that of another. It is given by:

$$\lambda_d = \sqrt{\frac{\varepsilon_0 \ k \ T_e}{n_e \ e^2}} \quad [6] \qquad \textbf{25}$$

where T_e is electron temperature and k is Boltzmann's constant (1.38×10^{-23} J K^{-1})

For typical values, λ_d is of the order 0.3mm suggesting a sheath length (d_s) of about 3mm.

Note: in practice the sheath appears to be slightly larger than this, perhaps up to 10mm.

This is very encouraging as plasma bulk can be seen in all circumstances to be perhaps 15–20cm and hence easily satisfies the condition $d_p < 400\ d_s$.

7. Suggestions for Further Work

Many areas of this subject have been covered and much learnt about the problems that are presented to methods of impedance measurement. Several approaches should be taken in the continuation of this work and are summarised below.

Standard loads

The accuracy of the complete calibration procedure revolves around the behaviour of the 50Ω and short circuit test loads. It is considered ideal to have these loads measured professionally and subsequently calibrated to eliminate any imaginary components. A similar measurement could be made on the various complex test loads in order for research to validate the probe and the appropriate model's performance. At this level of measurement the importance of accurate calibration standards is paramount.

Ideal shunt placement

The reasons behind shunt tuning have been discussed and shown to be favourable in terms of desensitisation of impedance measurements. However, there are practical constraints to achieving total cancellation of the electrode current due to the physical geometry of most chamber feed systems. A method is required in which shunt inductance can be placed directly at the electrode to form a perfect loop current by eliminating any loss. The difficulty with this arrangement is that the shunt inductance will be invasive to the behaviour of the plasma, hence very novel configurations will need to be considered.

Real-time Processing

Real-time processing is the type of requirement demanded by industry and would involve substantially more cost than the present system due to the cost of fast analogue to digital converters (ADC's). The price would still be very attractive in comparison to current available devices (Of the order of £6,000). Two methods are available.

Sample the signal directly

This requires a very fast ADC which will need to sample at rates of at least 10 Giga samples/sec (for 0.1ns resolution). Methods can be used to reduce this requirement such as random interleave sampling but the rate will still be high in terms of cost.

Down convert then sample

A more attractive proposal in which the signals from the probe are analogue mixed with an IF (intermediate frequency) on board the probe to produce a lower frequency version of the original. This can then be sampled at relatively low rates with increased precision of both time and amplitude parameters.

Whichever method is used it will allow a massive reduction in time for post development work as well as use in plasma research and the processing industry.

Impedance Modelling

There is various software available to model the behaviour of plasmas at the atomic level such as XPDP1 by Birdsall et.al. U.C. Berkeley. These simulations take a lot of time to run compared with a real discharge but they offer great insight into the behaviour of the various mechanisms. The RF voltage and current can be monitored together with impedance at any part of the RF cycle and this could be compared with measurements taken from a real system. The models normally used in this type of software are very simple and of symmetrical configuration therefore a real chamber would need to be developed that could be easily modelled to allow direct comparisons to be made. An important aspect of this work would be the ability to understand mechanisms that cause distortion in the current waveform that is monitored in either the real or simulated observations.

8. Conclusions

A method of determining the voltage and current at a fixed point along a transmission line has been devised. Calibration of such a device is paramount to the accuracy of any subsequent measurements, as are the procedure and model that are considered for the entire system.

Shunt tuning has been discussed in terms of its benefits with regard to eliminating sources of error due to the large electrode capacitance and it has been proposed that an accurate transmission line model be used to determine plasma parameters from those measured at the probe. The basis of this approach is to treat the entire feed system (from the two measurement points in the probe [V & I] to just ahead of the electrode), excluding the driven electrode, as a transmission line and characterise it completely. The line is characterised using an open circuit and short circuit impedance measurement. In this way the main error in the entire measurement system comes from a resistance measurement (to initially calibrate the probe) and a short circuit impedance measurement (to calibrate the feed system). Calibration will take into account feed and dielectric loss as well as the discrepancy concerning the point on the TX line the measurements are being taken. In this manner, the feed can be incorporated into the probe characteristics and effectively the point of measurement could be considered as the end of the transmission line i.e. the plasma itself.

Software has been written to Fourier analyse the V and I waveforms and to apply the TX line model to the measured data. The software has been used extensively with various complex loads, which has helped to validate the accuracy of the TX line model.

An argon discharge has been impedance analysed as a function of injected electron current with the results confirming theory in the main. However, this was performed with a simple RLC model used at the start of this work. Measurements taken with an accepted accurate TX line model as well as shunt tuning can only suggest more accurate determination of the plasma's impedance.

A lot has been learnt during this research and there is more to be confirmed. It is strongly believed that this final proposal for the system's analysis is the most accurate and secure method known at present.

9. References

[1] Sobolewski, M. 'Electrical measurements for monitoring and control of RF plasma processing', Proc. SPIE, vol, 1803, pp309-320, 1992

[2] Olthoff, J. et. al. 'The Gaseous Electronics Conference RF Reference Cell –An Introduction', Journal of Research of the National Institute of Standards & Technology, vol.100, No. 4, pp.327-335, August 1995.

[3] Edwards, T 'Foundations for microstrip design', Wiley, 1991 pp.51-54.

[4] Braithwaite, N. St. J. 'Internal and external electrical diagnostics of RF plasmas', Plasma sources Science Technology, Vol.6, 1997, pp.133-139.

[5] Sobolewski, M 'Electrical Characteristics of Argon RF Glow Discharges in an Asymmetrical Cell'. IEEE Trans. on Plasma Science, Vol 23. No.6. Dec 1995.

[6] Lieberman, M 'Principles of Plasma Discharges and Materials Processing' Wiley, New York, 1995.

[7] Topping, J. 'Errors of Observation and their Treatment' Science Paperbacks, Chapman & Hall.

[8] Dunlop, J. & Smith, D. 'Telecommunications Engineering', Chapman & Hall, 1989, p.184.

[9] Connor, F. R. 'Wave Transmission', Edward Arnold, 1972, p.15.

Appendix A

To measure the error in a value when several samples are taken it is not realistic to cascade the individual errors and present these to a value that is the function of measured parameters. Although, in theory a final error could be quite large (lots of small errors accumulating) a more realistic measurement is to consider the likely amount of error.

Using partial differentiation and from: -

$$(\mathrm{d}Q)^2 = (\frac{\mathrm{d}Q}{\mathrm{d}x}\Delta x^2) + (\frac{\mathrm{d}Q}{\mathrm{d}y}\Delta y^2) + ...[7] \qquad \textbf{A1}$$

Where the function may be $Q = AB$ or any other function
Taking the example $Q = AB$ and letting $A = x$ and $B = y$ we obtain: -

$$(\mathrm{d}Q)^2 = (B\Delta A)^2 + (A\Delta B)^2 \qquad \textbf{A2}$$

$$= (\frac{Q}{A}\Delta A)^2 + (\frac{Q}{B}\Delta B)^2 \qquad \textbf{A3}$$

Therefore: -

$$(\frac{\mathrm{d}Q}{Q})^2 = (\frac{\Delta A}{A})^2 + (\frac{\Delta B}{B})^2 \qquad \textbf{A4}$$

Rearranging: -

$$\mathrm{d}Q = Q\sqrt{(\frac{\Delta A}{A})^2 + (\frac{\Delta B}{B})^2} \qquad \textbf{A5}$$

In other words, the fractional error in Q is equal to the root of the sums of the individual fractional errors squared. For example, A and B could have 10% tolerance and Q 'could' have an error of 20% but the likely error is SQRT $[0.1^2 + 0.1^2] = 0.14$ i.e. 14% instead of 20%.

It can also be shown that equation 15 applies to division (Q=A/B) whilst error in Sum and Difference functions can be shown (in a similar manner) to be: -

$$\partial Q = \sqrt{(\Delta A)^2 + (\Delta B)^2 + ...} \qquad \textbf{A6}$$

It can be seen therefore that sum and difference functions concern only the error on components as opposed to product and quotient functions which are concerned with fractional errors.

Appendix B

Various test loads were used to validate performance of the probes. The following equations relate to two types of complex load in addition to the purely real 50Ω load.

R in series with C

$$|Z| = \sqrt{R^2 + (\frac{1}{\omega C})^2} \qquad \theta = -\arctan(\frac{1}{\omega C R}) \qquad \textbf{B1}$$

$$R = \sqrt{\frac{|Z|^2}{1 + (\tan\theta)^2}} \qquad C = \frac{1}{\omega R \tan\theta} \qquad \textbf{B2}$$

R in parallel with C

$$|Z| = \frac{R}{\sqrt{1 + (\omega CR)^2}} \qquad \theta = -\arctan(\omega CR) \qquad \textbf{B3}$$

$$R = |Z|\sqrt{1 + (\tan\theta)^2} \qquad C = -\frac{\tan\theta}{\omega R} \qquad \textbf{B4}$$

Appendix C

The Mk2 design is very different physically to the previous design in that it is designed using procedures similar to microstrip. This design is open (screened in Mk4 form) and consists of a rectangular slab of aluminium with N-type connector launches at each end and the main transmission line consisting of a 3mm track on a 1.6mm thick glass fibre PCB[3]. The line is then coated with silver loaded solder to reduce insertion loss. This design is inherently more stable against shock than the initial construction and the coupling of voltage to be a function of current (through the line) is achieved by a single parallel track to the main line.

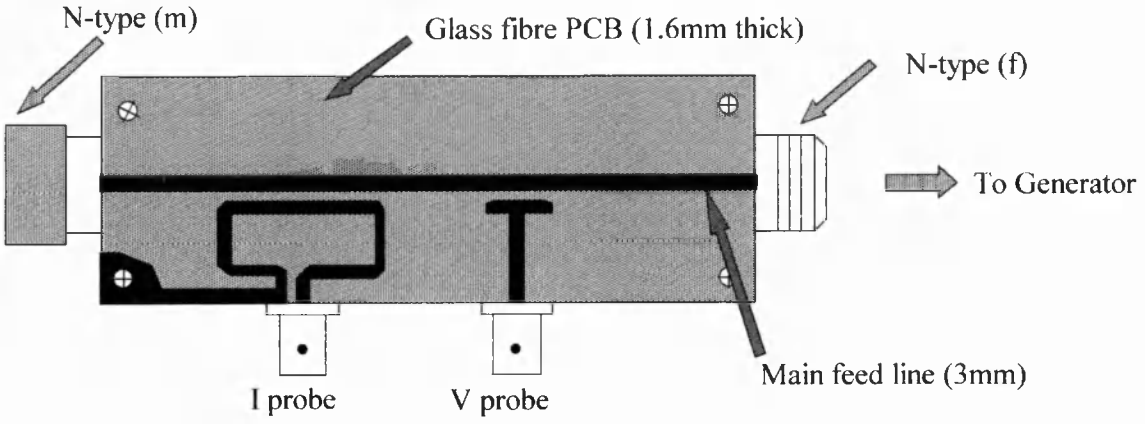

Figure C1. Mk2 VIPROBE design.

The probe is calibrated as usual and the following values are taken as the transfer functions. Since this probe was built, and various measurements taken, the Mk2 probe has now deceased. Mk3 and 4 probes have since been built in a similar manner.

Summary of the various probes.

Probe ver.	***V fact***	***I fact***	
MK 1	76.99	.748	Orig. Co-axial
MK 2	825	8.00	Deceased
MK 3	1998	24.3	Error in artwork
MK 4	1962	11.6	Enclosed design

Propagation delay for 2, 3 & 4, between measured signals, for an assumed real load is <0.2 ns.

The final version is pictured in figure C2 while placement of the shunt housing is shown in figure C3.

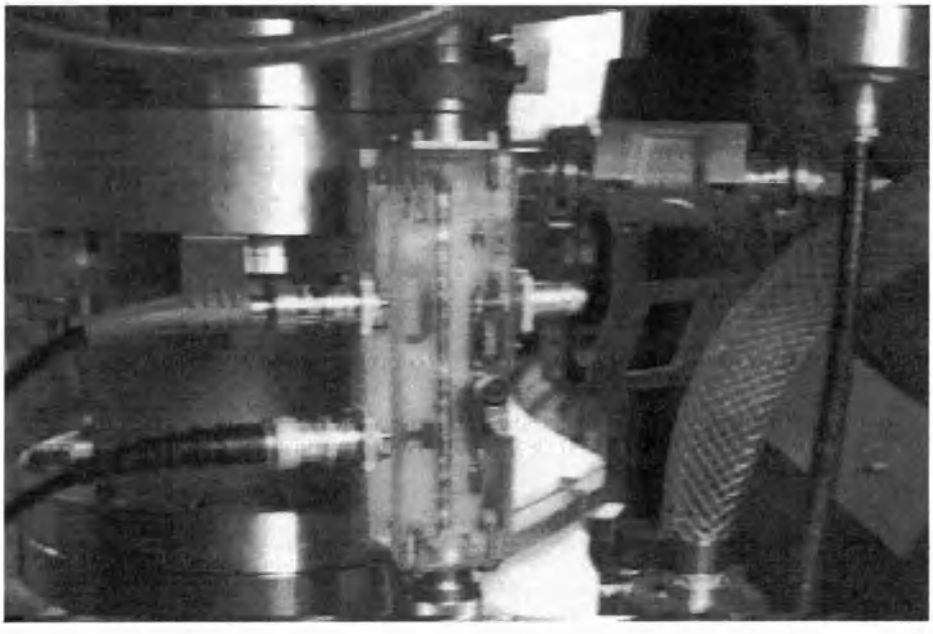

Figure C2. The Mk4 VI Probe, situated prior to the chamber feed.

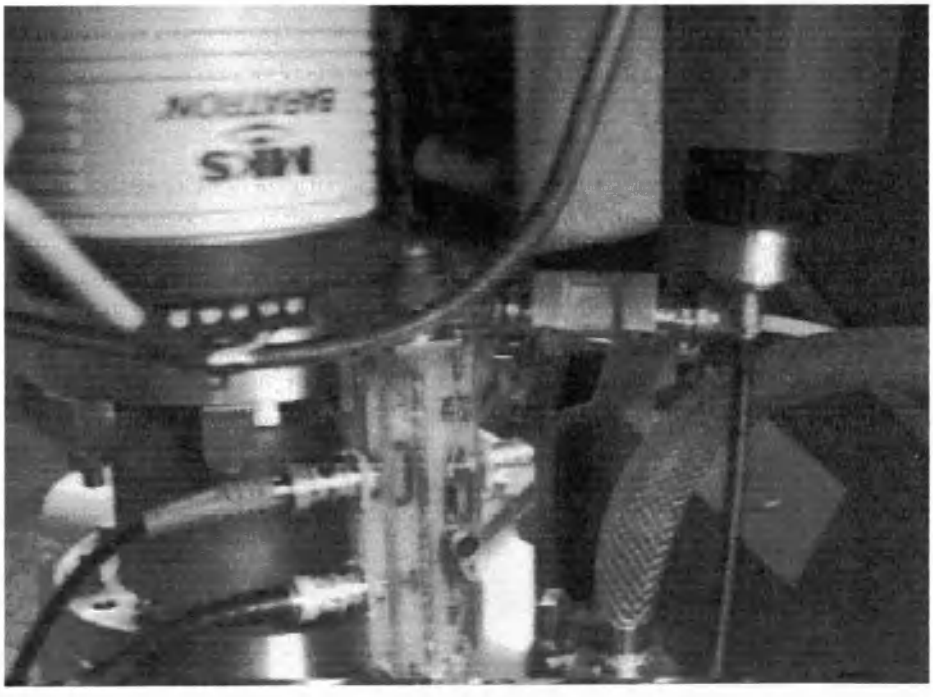

Figure C3. The VI Probe, in situ, with the shunt housing.

Appendix D

A visit was arranged to undertake work at and collaborate with the Physics Dept. Queen's University, Belfast. The work undertaken was performed in association with a Mr. Charlie Mahoney between the 14th and 16th of May 1997. The general opinion is that this work was a great success and invaluable to both parties.

Several parts of this research are now more fully understood and accepted as being appropriate to the discussed project.

Transmission Line Characteristics

The most important discovery is that the area of transmission line between the probe and the test load or plasma chamber cannot be ignored when it is not terminated in a matched condition. The length (and characteristic impedance) of the TX Line will affect the impedance looking into the line and the non-ideal load.

For a transmission line that exhibits loss, of length l and characteristic impedance Z_0, the voltage and current at the complex load as a function of those measured by the probe can be shown to be [8] :-

$$V_{load} = V_{probe} \cosh \gamma l - I_{probe} Z_0 \sinh \gamma l \qquad \textbf{D1}$$

$$I_{load} = I_{probe} \cosh \gamma l - \frac{V_{probe}}{Z_0} \sinh \gamma l \qquad \textbf{D2}$$

The propagation constant, $\gamma = \alpha + j\beta$. This is the complex sum of the attenuation (α) and phase coefficient ($\beta = 2\pi f / v_p$) of the wave on the line. Where v_p is the velocity of propagation within the medium and is directly related to the medium's relative permittivity.

$$v_p = \frac{c}{\sqrt{\varepsilon_r}}$$

Equations D1 and D2 can be rearranged and simplified to express Load impedance as a function of the measured V and I waveforms, Z_{probe}.

$$Z_{load} = \left(\frac{Z_{probe} - Z_0 \tanh \gamma l}{Z_0 - Z_{probe} \tanh \gamma l} \right) Z_0 \qquad \textbf{D3}$$

It can be shown [9] that:

$$Z_0 = \sqrt{Z_{o/c}\ Z_{s/c}} \qquad \textbf{D4}$$

$$\tanh \gamma l = \sqrt{Z_{s/c} / Z_{o/c}} \qquad \textbf{D5}$$

These are very important equations because they allow us to entirely characterise a particular TX line. Open and short circuit impedance measurements can be taken with a high degree of accuracy (using a shorting cap, figure 6 to determine $Z_{s/c}$) thus allowing us to determine V_{load} and I_{load} from the probe measurements.

Velocity of propagation can be estimated at about 2 x 10^8 m s^{-1} from having Teflon dielectric in the feed (ε_r = 2.1). Using this and knowing γl from the calibration, β, effective length (l) and α can be determined. However, this is not necessary to determine V, I and Z of the load.

Advantages

An important advantage of this calibration procedure is that it is not just the chamber feed that is being characterised, the probe is built about a TX line (of questionable effective length – V and I are not coupled at the same point) and therefore this is being included and hence accounted for with this procedure.

The effect of including the TX line model into the measurement of complex test loads is dramatic (even for 5cm of line) and the effectiveness of this calibration is highlighted in section 6.1 with some practical measurements.

Results from this characterisation can be equated with the model of a simple TX line, e.g. a lumped R, L and C network, to emphasise the importance of a distributed model that accounts for dielectric loss and wave propagation.

Inherent Errors due to Inductive Coupling

The current sensor in the form of an inductive loop is non-ideal in terms of its behaviour. The desired mutual inductance is accompanied by capacitance between the conductors. Generally it is accepted that current due to this is minuscule with respect to current induced from the inductance as the inductance is shorted to ground at one end (unlike the voltage probe).

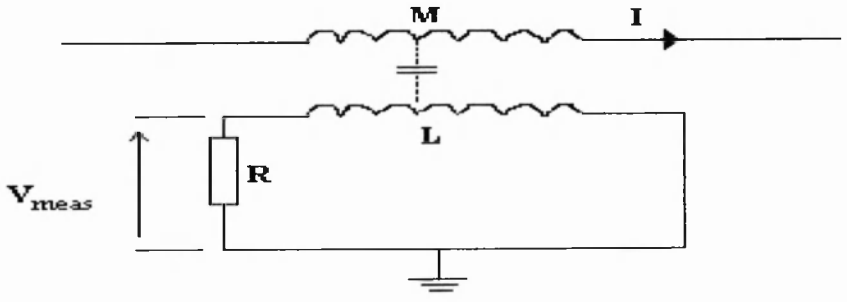

Figure D1. Current probe equivalent circuit.

In an ideal situation the voltage on the current probe is:-

$$V_{meas} = \left(\frac{R}{R + j\omega L}\right) j\omega M I \qquad \textbf{D6}$$

A more realistic expression is:-

$$V_{meas} = \left(\frac{R}{R + j\omega L}\right)(j\omega M I + V_{ind}) \qquad \textbf{D7}$$

Where L is the inductance of the loop, M is mutual inductance and V_{ind} is the voltage induced in this network due to the voltage on the line and the capacitive coupling between them.

Equation D7 is an approximation to a lumped network where in reality the coupling capacitance is distributed. This model is used only to consider the effect this capacitance may have on the accuracy of results. With typical values it can be shown that V_{ind} is a couple of orders smaller than the voltage induced from current and can therefore be considered negligible.

It should be noted however that inaccuracies due to this will increase with increasing load impedance. A high load impedance relates to small current and high voltage on the line and therefore impedance's >> 1000 ohms can cause significant errors in the current measurement.

Other Useful Ideas

The following types of coupler configuration have been discussed as worthy of investigation/development.

i) Coupling the voltage and current at the same point on the line would reduce phase error to a theoretical 0° (at present, with about 3cm between them, the phase difference for a real load is approaching 0°, in the region < .3°).

ii) At present the voltage coupler has a capacitance to the main line in terms of a direct path and via their common ground planes. The signal from the voltage coupler 'head' is therefore attenuated by it's large capacitance to ground (the head is not matched to 50Ω) and consequently signal is lost which means inefficient voltage detection. If a channel is milled out of the ground plane underneath just the voltage head then it need not be so close to the main line for the same coupling, reducing the probe's insertion loss.

iii) Another idea worth considering is to have the main probe line split into two and then joined back into one, as in conventional microwave power splitters/ combiners. The voltage and current probes could then be placed at the same point along the travelling wave, as suggested in **i)**, but the distance between them should resolve any discontinuities caused by coupling between the two.

Tailoring of Particle Energy Distributions in Low Temperature Plasmas

A. Goodyear, J. P. Moore, P. Godinat, and N. St. J. Braithwaite

The Open University, Oxford Research Unit, Oxford, OX1 5HR, UK

The efficiency and effectiveness of plasma processing benefits from a greater degree of control over the physical and chemical interactions in the plasma, especially those at and near surfaces. The electron energy (distribution eedf) influences directly the gas phase processes and indirectly the ion energy distribution (iedf). This work investigates the electrical tailoring of the eedf so that more effective use can be made of particular plasma sources. This is achieved by injecting extra electrons into the plasma; injection flux and energy are important new control parameters[1]. In particular we have shown that injecting electrons changes potential structure[2] and the balance of the energy exchange processes responsible for sustaining of the steady eedf; as a result the eedf and iedf are altered[3,4]. The ionization balance is also disturbed and higher plasma densities can be achieved[2,3]. These changes are reflected in an altered impedance of the plasma[5,6]. Results are presented for 13.56 MHz plasmas in argon and other gases at 1-100 Pa.

Aim

To develop strategies for electrical control of low pressure plasmas

Objectives

1. To make substantial adjustments to the eedf in RF plasmas
2. To make substantial adjustments to the iedf in RF plasmas

Work supported by the EPSRC, Grant No. GR/K58067

1

Experimental System

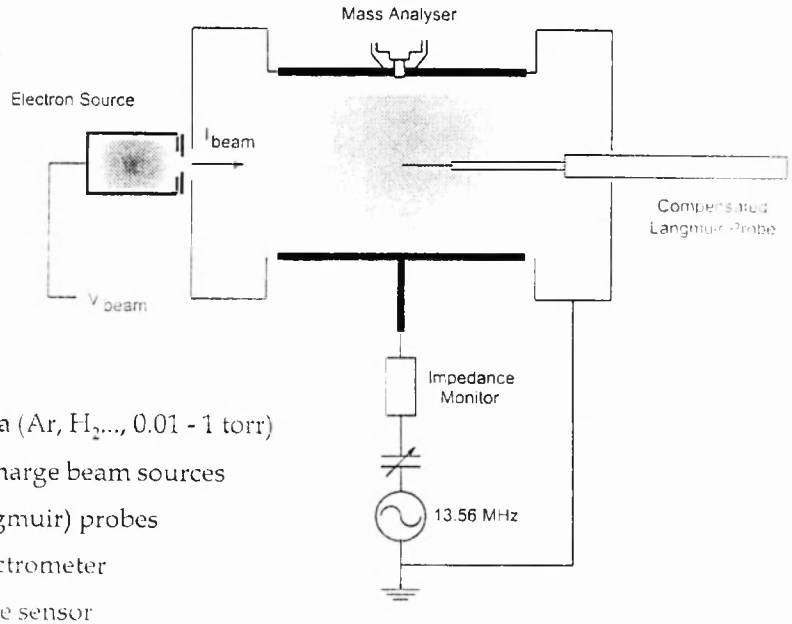

- 13.56 MHz plasma (Ar, H_2..., 0.01 - 1 torr)
- filament and discharge beam sources
- electrostatic (Langmuir) probes
- mass/energy spectrometer
- plasma impedance sensor

2

Plasma Modification

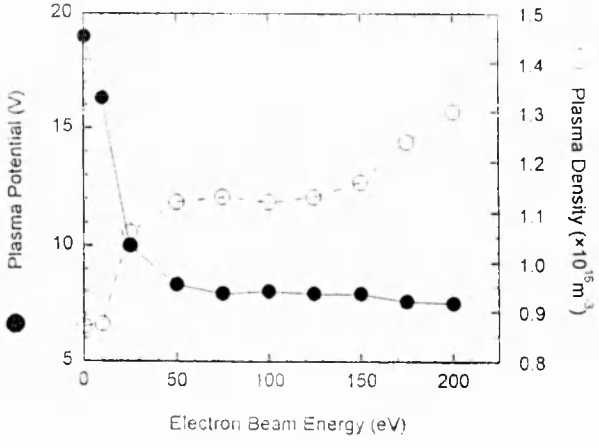

Injection of variable energy 80mA electron beam into a 20mTorr,.25W, 13.56 MHz argon plasma.

Note that the plasma potential can be decreased independently of density if the beam energy is maintained below the ionisation threshold of the argon gas (15.8eV).

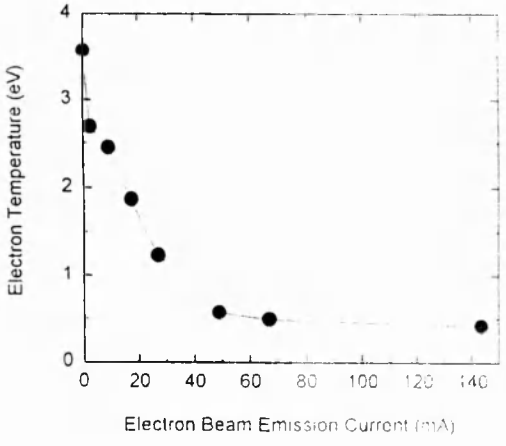

Depression of electron temperature of plasma EEDF by 80eV electrons injected into a 46mTorr, 30W, 13.56 MHz hydrogen plasma.

3

Electron Energy Distributions

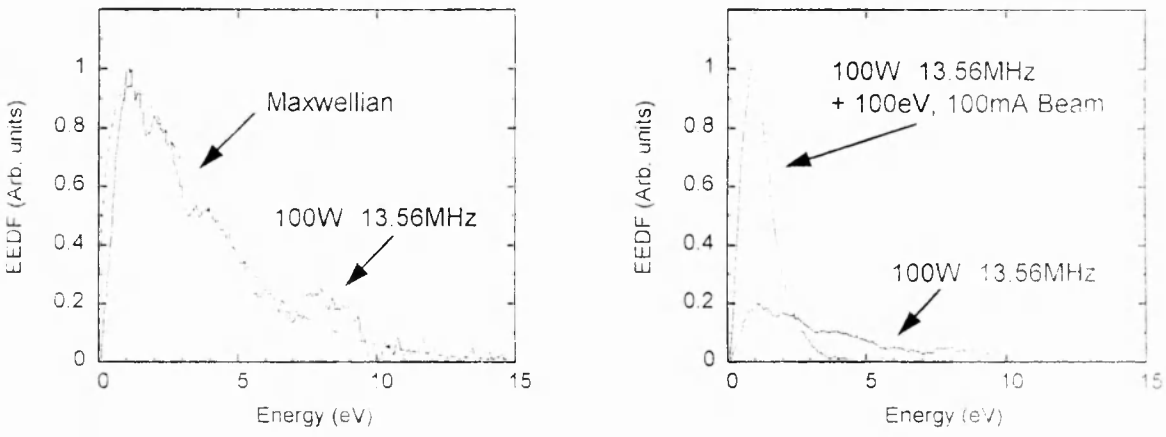

Electron Energy Distribution Functions (EEDFs) for a 100W, 20mTorr argon plasma and the same plasma with the injection of a 100eV, 100mA electron beam.

4

Ion Energy Distributions

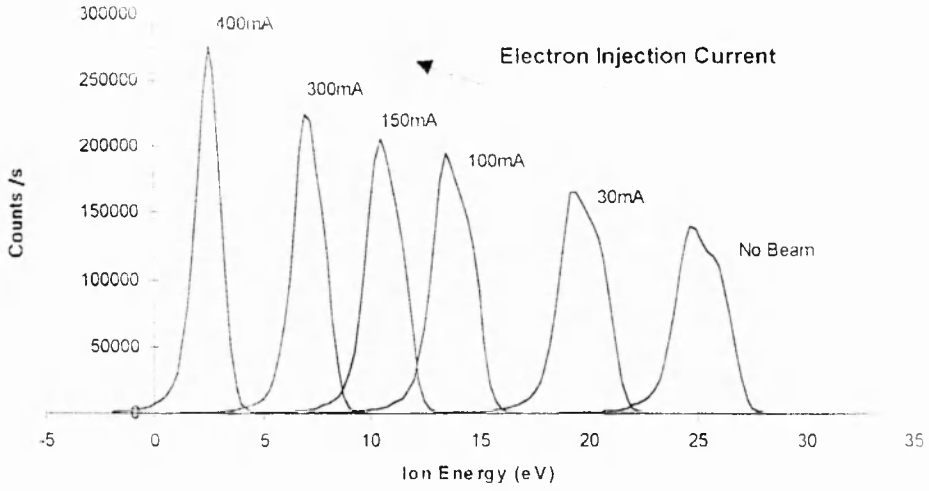

H_2O^+ Ion Energy Distributions in a 80mTorr, 120W, 13.56MHz Argon plasma with Electron Injection

5

Impedance Probe

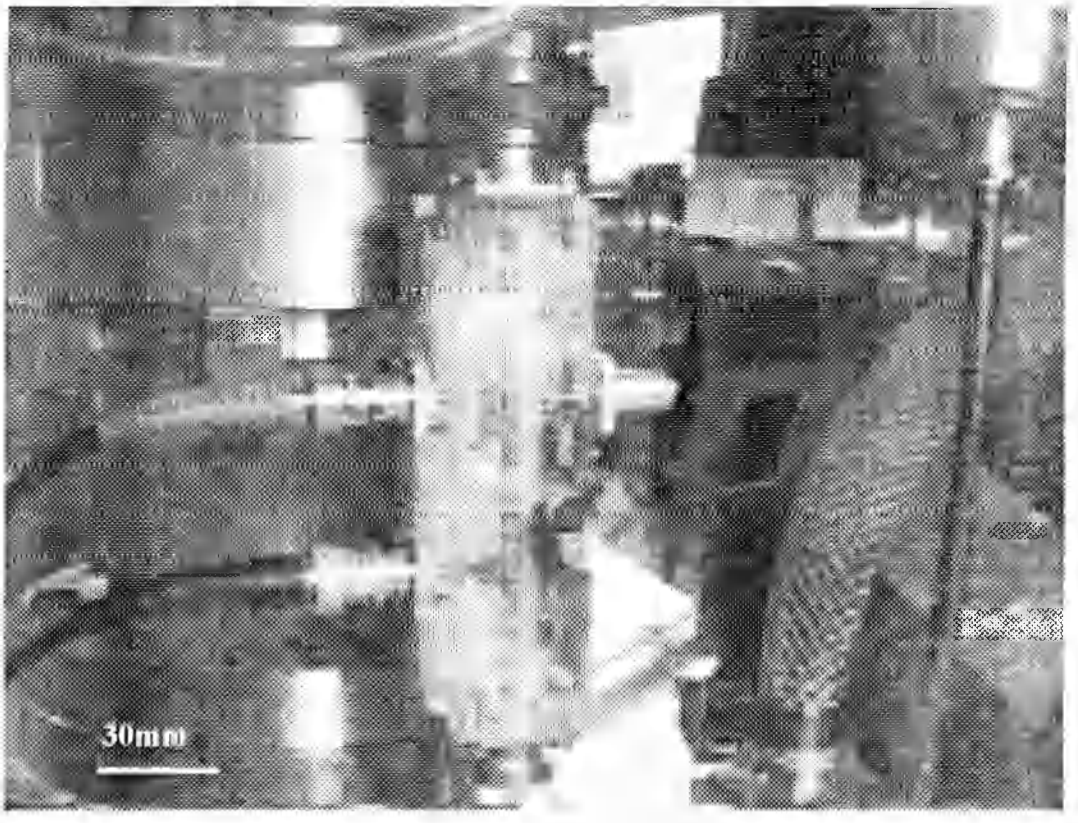

Voltage and current probe shown under the RF discharge chamber and situated in line of the main electrode's feed.

The voltage and current waveforms are determined from capacitive and inductive coupling respectively from the main line.

Transfer functions of these coupling functions are calculated from calibration of the probe using precision standard loads.
(50W, $Z_{\text{open circuit}}$ and $Z_{\text{short circuit}}$)

6

Discharge Impedance

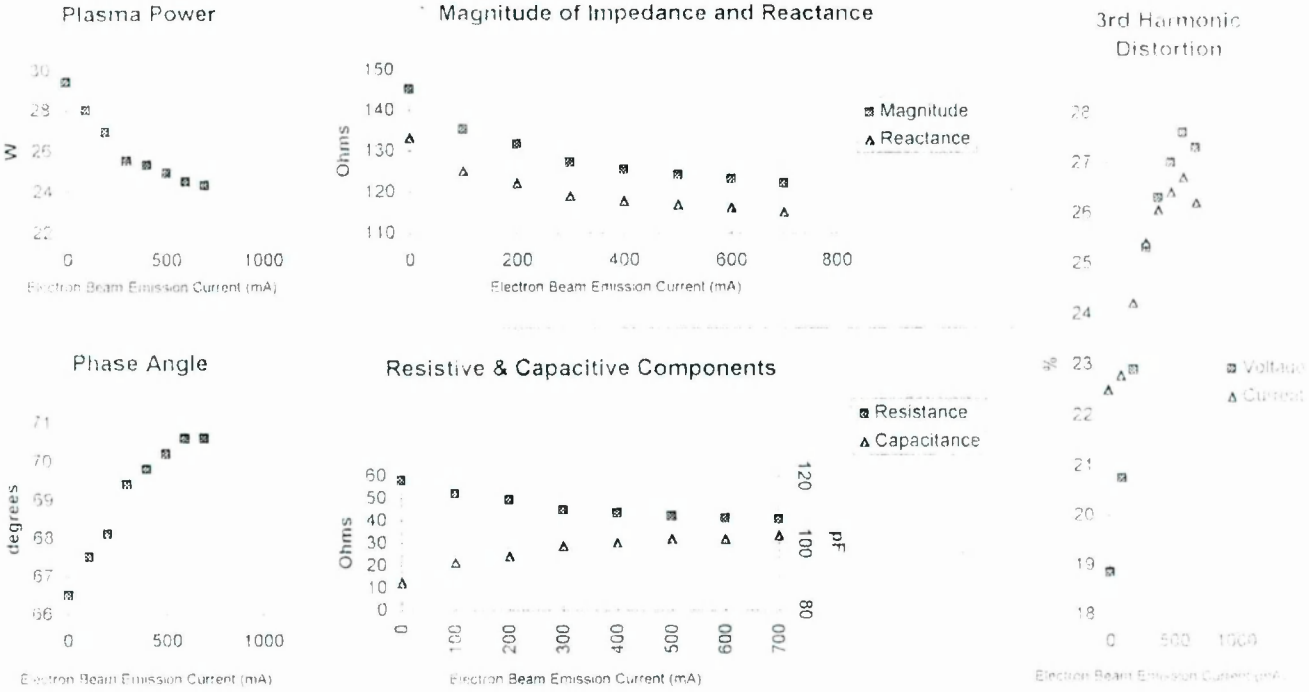

Power, Impedance & Distortion measurements of a 20mTorr Argon Discharge excited from a nominal 30W 13.56MHz RF source

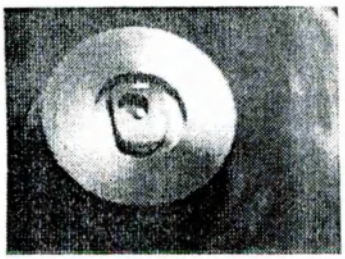

Conclusions

Modulation of an RF plasma by a DC electron beam can lead to substantial changes in the particle energy distributions.

- eedf $\Leftrightarrow n_e$, "kT_e"
- iedf $\Leftrightarrow V(x)$, "kT_e", n_i
- $Z_p \Leftrightarrow$ eedf